WORKSHOP ON CAVITATION EXPLOITATION 2023 - PROGRAM

20th – 22nd of September 2023

Ljubljana | Slovenia

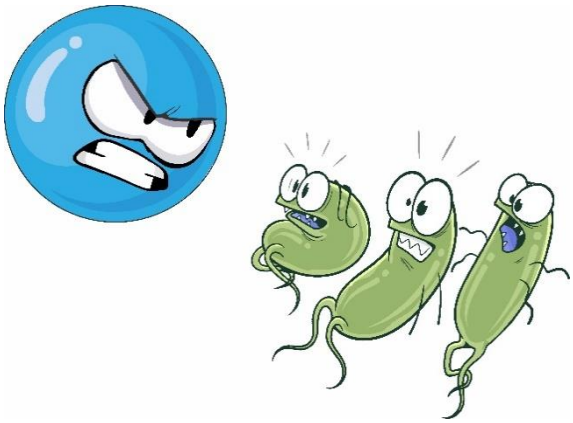

University of Ljubljana
Faculty of Mechanical Engineering

European Research Council

PROGRAM

WEDNESDAY, 20. 9. 2023

08:50 Opening address: Matevž Dular

09:00 Keynote: Claus Dieter Ohl: *Cavitation meets hard and soft matter*

09:45 Tadd Truscott: *Cavitation by low-speed water impact*

10:05 Jurij Gostiša: *On the path to Pin Disc Hydrodynamic Cavitation Reactor commercialisation*

10:55 Iakovos Tzanakis: *Ultrasonic Cavitation Processing of Multi-functional Materials: Fundamentals and Applications* (Virtual talk)

11:15 Yatha Sharma: *Bulk Nanobubble Generation from Laser-heated Gold Nanoparticles*

11:35 Haley Kuhn: *Characterization of Ozone Nanobubble Technology (NBOT)*

11:55 Peter J. Thomas: *Concept for investigating effects of Coriolis forces on cavitation bubble collapse*

12:15 Evangelos Koukas: *Numerical investigation on cavitation induced blood vessel injury during ultrasound treatments*

13:05 Keynote: Mojca Zupanc & Martin Petkovšek: *Cavitation exploitation beyond the scope of CABUM*

13:50 Iryna Koval: *Ultrasound cavitation of microbial water*

14:10 Francesco Meneguzzo: *Preliminary Patterns and Quantitative Assessment*

15:30 Keynote: Giancarlo Cravotto: *Cavitational chemistry and processing the truth about real industrial applications*

16:15 Arijana Filipić: *Cavitation alone or in combination with plasma for waterborne virus inactivation*

16:35 Pavel Rudolf: *Device for water disinfection based on cavitation and cold plasma discharge*

16:55 Uroš Tkalec: *Water droplet impact on thin liquid crystal films*

THURSDAY, 21. 9. 2023

09:00 Keynote: Timothy Leighton: *Difficult questions on the nature of cavitation exploitation*

09:45 Adriano Troia: *Piezocatlysis from ultrasonic irradiation of simple inorganic salts*

10:05 Takaomi Kobayashi: *High frequency ultrasonic water stream for cleaning processes*

10:55 Robert Mettin: *Ultrasonic degassing - some facts and mysteries* (Virtual talk)

11:15 Hendrik Resse: *Rayleigh wave induced cavitation*

11:35 Christiane Lechner: *Bubble collapse at a solid boundary: influence of bubble size, liquid viscosity and ambient pressure on jet formation*

11:55 Hemat Sagar: *Cavitation bubble dynamics near brittle boundaries*

12:45 Keynote: Judy Lee: *The Art of Sonocrystallisation*

13:30 Fabian Reuter: *Non-invasive pressure measurement on the collapse of single erosive cavitation bubbles*

13:50 Jure Zevnik: *Cavitation bubble interaction with compliant structures on a microscale*

14:10 Jaka Mur: *Optical methods for detection and evaluation of cavitation bubbles and accompanying phenomena*

15:30 Žiga Pandur: *Effect of cavitation microbubble on individual bacterial cells*

15:50 Deepak Kumar Pandey: *Micro-scale processes in cavitation-induced drop breakage*

16:10 Morteza Ghorbani: *2D Nanomaterials Exfoliation in Hydrodynamic Cavitation on Chip*

16:30 Dominik Mnich: *Single cavitation bubble dynamics and erosion in a stagnation flow*

16:50 Luka Kevorkian: *Experimental investigation of cavitation-induced removal of paint from the surface of the Venturi channel*

FRIDAY, 22. 9. 2023

09:00 Keynote: Grzegorz Bozickaj: *Advanced treatment of water and wastewater by physio-chemical processes aided by cavitation – recent developments and challenges*

09:45 Frank Rüdiger: *Some aspects of similarity and transferability for processes with hydrodynamic cavitation*

10:05 Matej Praprotnik: *DPD Simulation of Ultrasound Propagation through Liquid Water*

10:55 Xiaoge Wu: *Study on the behavior of cavitation bubbles on the surface of nanodiamond in the ultrasound field for Microcystis aeruginosa removal* (Virtual talk)

11:15 Avinash Kumar: *Towards the concept of early detection of atherosclerosis using ultrasound contrast agent*

11:35 Mazyar Dawoodian: *Hydrodynamic process of droplet generation using spark bubble cavitation*

11:55 Žan Boček: *The beginning of the ultrasonic emulsification process*

12:15 Suat Canberk Ozan: *A hybrid Eulerian-Lagrangian CFD model for predicting cavitation intensity*

12:35 Closing Remarks: Matevž Dular

KEYNOTE SPEAKERS

WEDNESDAY, 20. 9. 2023

Claus-Dieter Ohl (Germany)

Prof. Claus-Dieter Ohl has graduated with a PhD in physics in 1998 in the group of Prof. Werner Lauterborn from Göttingen University. He then spent time as a postdoc with Prof. Andrea Prosperetti, at Johns Hopkins University, Prof. Detlef Lohse at Twente University, studying mostly bubbles in liquids with experiments. From 2005 he became group leader on bioeffects of cavitation as VIDI fellow. In 2007 he joined as Assistant Professor Nanyang Technology University in Singapore. The research remained with vapor and gas bubbles, but it also extended towards the surface nanobubbles. In 2021 Prof. Ohl was tenured and he joined in 2017 the Otto-von-Guericke University in Magdeburg as full professor. Current interest are cavitation in soft material, bulk nanobubbles, and surface waves.

Mojca Zupanc (Slovenia)

Res. Assoc. Dr. Mojca Zupanc is a researcher at the University of Ljubljana in the field of cavitation exploitation, where she focuses on connecting basic science with real-world applications. After receiving her PhD in 2013 in the field of environmental science, where she studied the potential of cavitation for the degradation of micropollutants. She was awarded the Excellence in Science Award in 2022. Her innovative work in developing various cavitation devices resulted in two second prizes in the Best Innovation Award competition at the University of Ljubljana (2014 and 2022), a grant from the University of Ljubljana Innovation Fund (2020), UL Knowledge Transfer Office, for projects with industrial use potential, a national patent (SI 24180 A, 2014), and two international patent applications (LU501013: 2021; WO2022112191A1: 202). She is also a PI in a bilateral Slovenia-Turkey project (2023-2024).

Martin Petkovšek (Slovenia)

Assist. Prof. Dr. Martin Petkovšek is a researcher at the University of Ljubljana. He is specialized for research in fluid dynamics and two-phase flows, with emphasis on cavitation. His field of expertise is experimental modeling of cavitation erosion, thermodynamic effects at cavitation, exploitation of cavitation for (waste)water treatment and basic research on cavitation dynamics. He received his PhD in 2016 and was appointed Assistant Professor in 2018. As a visiting researcher, he worked at ParisTech (France), VirginiaTech (USA) and University of Twente (Netherland). He has published more than 35 journal articles and co-authored 4 patents. For his innovative work he was awarded 2nd prize (together with M. Dular and M. Zupanc) at the "Best Innovation Award" of the University of Ljubljana (2014) and 1st prize (together with M. Dular) at the International Technology Transfer Conference of the Jozef Stefan Institute (2020). As principal investigator he received funding in total of 1M EUR for 4 research projects.

Giancarlo Cravotto (Italy)

Giancarlo Cravotto became a researcher at the Department of Drug Science and Technology (University of Turin), after four years of experience in the chemical and pharmaceutical industries. His research activity in the domain of green organic synthesis and processing, is documented by more than 500 scientific, peer-reviewed papers (H. Index 63, 17,000 citations by Scopus), 21 patents, 42 book chapters and 7 books as editor. He is Full Professor of Organic Chemistry and Department vice-Director (former Director 2007-2018). He is Editor-in-Chief of Processes (MDPI) and former ESS President (European Society of Sonochemistry). Recent Awards: Gold medal "Paternò" 2020 (Italian Chemical Society).

THURSDAY, 21. 9. 2023

Timothy Leighton (United Kingdom)

Timothy Leighton FRS FREng FMedSci ScD is the founder and Chair of the Global Network for AntiMicrobial Resistance and Infection Prevention (Global-NAMRIP). He is Professor of Ultrasonics and Underwater Acoustics at the University of Southampton; and the Executive General Director and Inventor-in-Chief of Sloan Water Technology Ltd., a UK manufacturer and R&D establishment founded on his patents. A fellow of three National Academies, he has been awarded 8 international medals, and 6 international prizes. His fundamental discoveries have lead to changes in practice, and the introduction of new technology, for ocean and space exploration; for climate change prediction; for infection prevention and pandemic research; for the safety of human exposure to ultrasound; for marine mammal communications and behaviour; for the treatment osteoporosis, kidney disease and migraine; and for advanced radar and sonar. The Institute of Physics Paterson medal citation (2006) describes "*Timothy Leighton's contribution is outstanding in both breadth and depth. He is an acknowledged world leader in four fields*".

Judy Lee (United Kingdom)

Judy Lee obtained from Melbourne University, Australia: a degree in B.Eng. (Chemical) and B.Sc (Physics), and PhD on "Acoustic bubble dynamics in the presence of surfactants". She spent 1.5 years as a postdoc on "Ultrasonic processing of dairy ingredients", 2 years as a JSPS Fellow in Japan exploring "Acoustic cavitation dynamics and production of functional shelled-microbubbles" and to diversify her research area, she spent further 2 years as a postdoc on membrane filtration for desalination. In 2012 she was awarded the DECRA by the Australian Research Council to work on "Ultrasound enhanced crystallisation". In 2015 she joined Surrey University UK as a Senior Lecturer and promoted to Associate Professor in 2021, and is currently Director of Learning and Teaching for Chemical Engineering. Her research interests are fundamental and applied aspects of ultrasound processing and membrane filtration, with a particular interest in water and wastewater treatment.

FRIDAY, 22. 9. 2023

Grzegorz Boczkaj (Poland)

Grzegorz Boczkaj is an associate professor at the Faculty of Civil and Environmental Engineering, Gdansk University of Technology (GUT), Poland. He obtained a PhD (2012, with honors) in chemical technology (chemical engineering) at GUT and a habilitation in same discipline (2017). He is the leader scientist of research group working on new developments in the field of environmental science, separation techniques, chemical engineering as well as analytical chemistry. He was a principal investigator of several research projects (in total above 1,5 mln $). Few projects were dedicated to studies on fundamentals and applications of cavitation based processes. He has published over 150 journal articles, book chapters, and technical reports.

ABSTRACTS

On the path to Pin Disc Hydrodynamic Cavitation Reactor commercialisation

Jurij Gostisa [1], Matevz Dular[1], Tadej Stepisnik[2], Mojca Zupanc[1]

[1]*Faculty of Mechanical Engineering, University of Ljubljana*
[2]*National Technical University of Athens*

Abstract

An energy-efficient, large capacity and robust hydrodynamic cavitation (HC) generator is one of the key missing elements on the way to the industrial exploitation of HC. One promising type of such device is the rotating HC generator, which is the focus of our research. Our group has been working in the field of cavitation utilisation for more than 10 years, and we have reached a point where we want to advance the science toward commercialization, and to do this we needed to achieve three main goals. First, we had to find an industrial process for a "problematic" fluid where cavitation could be used in an economically acceptable way. Second, we had to develop a machine – the cavitation generator - that could efficiently perform the set task and finally, we had to acquire at least basic entrepreneurial skills to handle the commercialization part. We found that the substrates used to produce biogas in the anaerobic reactors could be pretreated with cavitation to make the nutrients more accessible to the bacteria and improve production yield and speed. We are currently in the pilot testing and economic feasibility evaluation phase.

Effect of Particle Size on Laser Nucleation of Bulk Nanobubbles on Gold Nanoparticles

Yatha Sharma[1], Claus-Dieter Ohl[1], Juan Manuel Rosselló[1,2]
[1]*Otto-von-Guericke-University Magdeburg, Institute of Physics, Universitätsplatz 2, 39106 Magdeburg, Germany*
[2]*Faculty of Mechanical Engineering, University of Ljubljana, Askerceva 6, 1000 Ljubljana, Slovenia*

1. Introduction

Gold nanoparticles absorb light in the visible spectrum. Due to the high electrical conductivity of gold and the particle sizes below the wavelength of the light, plasmonic resonance may occur. When the resonance conditions are met, the particles heat up, and subsequently, the excess of heat dissipates to the surrounding medium. This energy transfer potentially induces a localised liquid-gas phase transition, leading to the formation of vapour bubbles in immediate proximity to the nanoparticles. The heat transfer from the particles to the liquid bulk is influenced by factors like the duration of the excitation laser pulse, laser pulse fluence, nanoparticle size, and the material of the nanoparticles, etc. [1].

2. Objectives

This research focuses on studying the effects of critical parameters such as laser pulse energy, particle size, and solution concentration on the formation of vapour nanobubbles through laser energy deposition on gold nanoparticles suspended in a solution.

3. Materials & methods

The experimental setup for pulsed laser-induced bulk nanobubble generation is shown in Fig. 1(a). The nanobubbles are created when the particles in the liquid sample are illuminated by a collimated laser beam (Nd:YAG) with a wavelength of 532 nm. The samples are contained in a glass cuvette placed on top of a shockwave generator (medical-grade Lithotripter) as shown in Fig. 1(a). The lithotripter creates a shock wave followed by a rarefaction wave (Fig. 1(b)) which is focused in the path of the the laser beam [2,3,4].

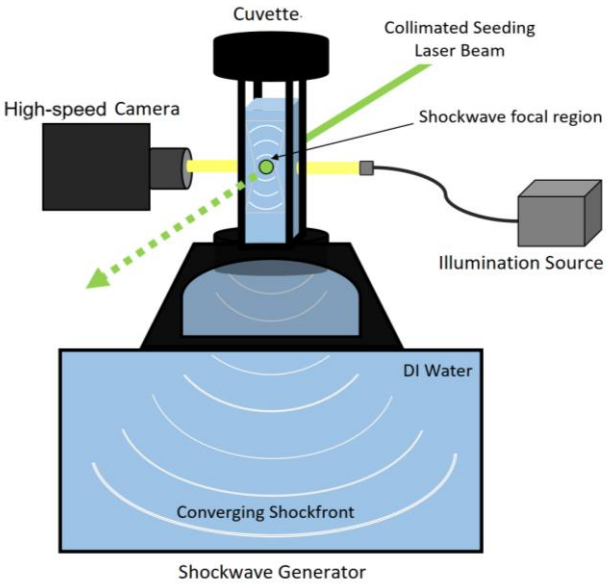

Figure 1(a): Experimental setup (side view)

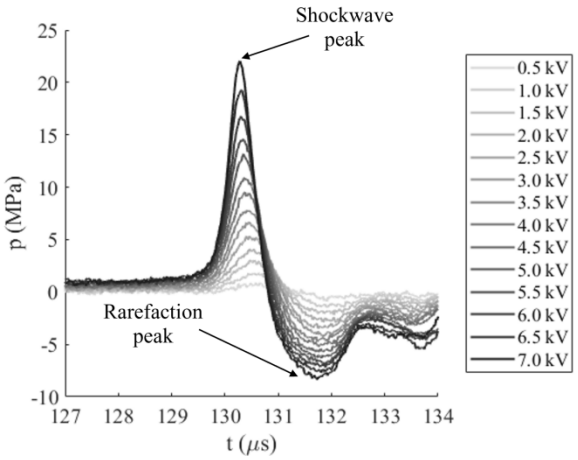

Figure 1(b): Shockwave generator bipolar pressure curves

The negative phase of the pressure wave expands the nano-sized voids into micron-sized bubbles for a short duration. These are then illuminated by a continuous LED light source and observed orthogonally to the laser beam using a high-speed camera. The image pixels are about 10.9 μm in size.

Nanobubble nucleation was studied in four different liquid samples. The control sample (i.e., ultrapure water passed through a 50 nm pore size filter, here called nanopore water, NPW) was compared with different solutions of gold nanoparticles of 10, 60, and 150 nm in diameter and concentrations of ~ 10^3 and ~ 10^4 particles/ml.

4. Results

The nucleation efficiency (see Fig. 3) of gold nanoparticles of different sizes was computed by comparing the bubble population generated by the nanoparticles in a given nucleation volume to the estimated number of added nanoparticles in that volume. The nucleation volume (as shown in the inset of Fig. 2) was calculated based on the frame width where the bubble nucleation occurs. This width was treated as the diameter of an imaginary cylinder, in which the laser energy exceeds the nucleation fluence threshold.

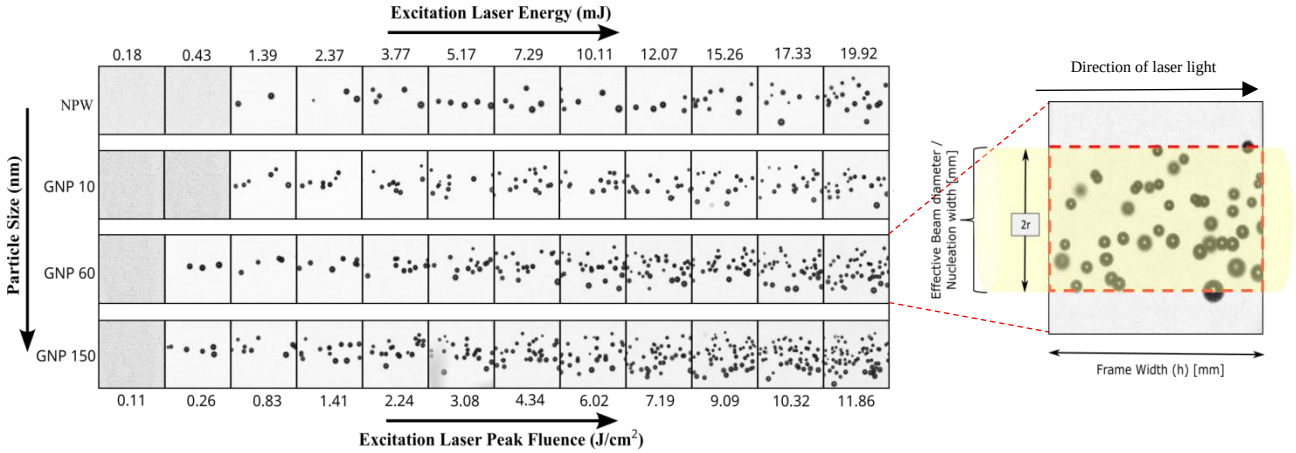

Figure 2: Left: bubble population at different laser energies and particle sizes; right: example image with nucleation width

The influence of the nanoparticle size on the dynamics of nanobubble dissolution was also studied as a function of delay times (Δt) between the seeding laser pulse and the arrival of the rarefaction wave in the test samples (see Fig. 4). The change in the bubble number as a function of Δt was then correlated with the theoretical dissolution time derived from the Epstein-Plesset model.

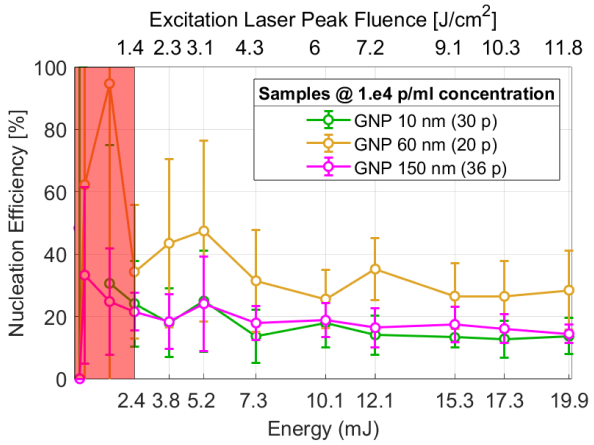

Figure 3: Effect of laser energy on the nucleation efficiency

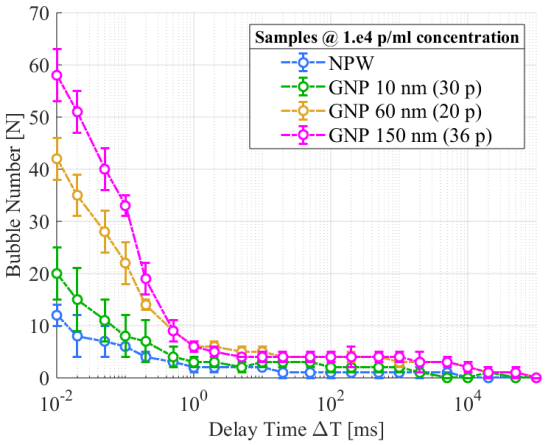

Figure 4: Lifetime of nanoparticle-based nanobubbles

5. Conclusions

Varying the laser energy showed no significant effect on the nanobubble nucleation efficiency of the nanoparticles. The deviations in the data at energy densities lower than 1.41 J/cm² (shown in red) are due to small nucleation volumes and can be omitted from the analysis. The bubble nucleation efficiency is highest for a particle size of 60 nm. However, the nanoparticle size did not significantly affect the size and lifespan of the generated nanobubbles.

References

1. Hashimoto, S. and Uwada, T. (1970) 'Laser-induced bubble generation on excitation of gold nanoparticles', *SpringerLink*. doi: 10.1007/978-981-16-7798-4_1.
2. Rosselló, J. M. and Ohl, C.-D. (2021) 'On-Demand Bulk Nanobubble Generation through Pulsed Laser Illumination', *Physical Review Letters,* 127, 044502. doi: 10.1103/PhysRevLett.127.044502
3. Rosselló, J. M. and Ohl, C.-D. (2023) 'Clean production and characterization of nanobubbles using laser energy deposition', *Ultrasonics Sonochemistry*, 94, p. 106321. doi: 10.1016/j.ultsonch.2023.106321.
4. Jelenčič M, Orthaber U, Mur J, Petelin J, Petkovšek R.(2023) 'Evidence of laser-induced nanobubble formation mechanism in water', *Ultrasonics Sonochemistry,* 99, doi: 10.1016/j.ultsonch.2023.106537.

Characterization of Ozone Nanobubble Technology (NBOT)

H. E. Kuhn[1,2,3], W. P. Fagan[1], J. D. Fuchs[1], L. K. Weavers[1,2,3]

[1] *Civil, Environmental and Geodetic Engineering, Ohio State University, Columbus, OH*
[2] *Environmental Sciences Graduate Program, Columbus, OH*
[3] *Ohio Water Resources Center, Columbus, OH*

1. Introduction

Ozone is a powerful oxidant that has been used in water treatment for over a century[1]. Ozone reacts with contaminants via direct oxidation by molecular ozone (O_3) and through hydroxyl radicals (•OH) produced during ozone decomposition. Ozone is an unstable gas; therefore, it is produced on-site and delivered to water as a gas. Today, ozone is typically delivered via macro-sized gas bubbles in water treatment, but the use of nanobubbles is emerging. Nanobubbles are bubbles with diameters smaller than 1 µm. The small size of nanobubbles provides favorable characteristics for gas delivery into water, including reduced buoyancy resulting in a longer lifetime in aqueous solutions, higher mass transfer, and minimized off-gas from solution[2]. Additionally, previous work suggests that nanobubbles produce •OH during collapse, which would provide additional oxidation. Nanobubble ozone treatment (NBOT) delivers ozone gas through nanobubbles, which may increase the effectiveness of ozone treatment[3,4]. This research was completed as part of a larger study examining the effectiveness of NBOT for the treatment of cyanobacteria harmful algal blooms. Here, we aim to characterize O_3 and •OH formation, characteristics, and lifetime during NBOT treatment.

2. Objectives

The objective of this study is to determine the oxidants produced within the system during NBOT treatment, and at what quantity. Specifically, objectives are:

1. Quantify aqueous O_3 produced during and after treatment.
2. Quantify •OH production during and after treatment.
3. Determine O_3 fate and formation of •OH through the unit.

3. Materials & methods

The NBOT unit used in this study consists of an ozone generator attached to a pump system that produces and delivers ozone nanobubbles into solution (Figure 1). An oxygen concentrator feeds an ozone generator(s) which injects ozone into the influent, untreated water via a venturi system. Then, effluent ozonated water flows into a contact tank equipped with an ozone destruct mechanism to eliminate released gaseous phase ozone. Water is pumped out of the system under constant pressure through a patented nozzle that creates additional nanobubbles. The ozone generator can be turned off, allowing for experiments with oxygen nanobubbles to be conducted as well.

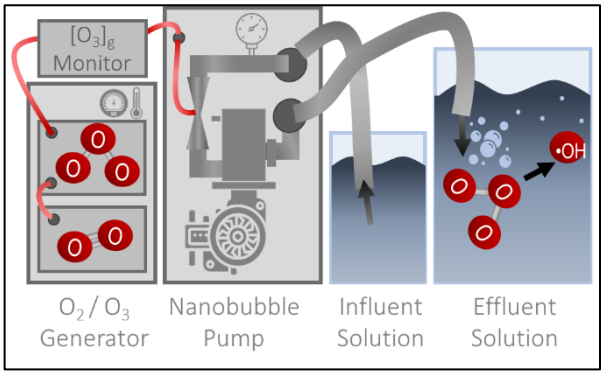

Figure 1. Diagram of the Nanobubble Ozone Technology unit.

To determine aqueous ozone concentration, indigotrisulfonic acid (indigo) with an absorbance at 600 nm was used[5]. At a low pH (pH < 3), ozone reacts with the carbon-carbon double bond in indigo, resulting in a bond cleavage that produces colorless products which do not interact further with ozone. The change in indigo absorbance is proportional to the concentration of aqueous ozone, and thus is used to determine the aqueous ozone concentration produced during treatment.

To measure •OH production, disodium terephthalate (TPT) was used as a probe. TPT is a nonfluorescent molecule that reacts with •OH to produce hydroxyterephthalate (HTA), a

fluorescent molecule[6]. The increase in fluorescence intensity is proportional to the cumulative concentration of •OH produced. This method works over a range of pH, allowing for these experiments to be completed at low (< 3) and high (> 8) pH.

These probes were used to determine the mass transfer, formation, and fate of oxidants produced during NBOT treatment. To quantify the production of oxidants within the NBOT unit, the probes were added to a buffered DI influent solution and pumped through the unit. Probes were also added to buffered DI effluent solution to determine the formation and fate post treatment. The change in fluorescence/absorbance was also measured over time to calculate the cumulative formation of the oxidants.

4. Results and Conclusions

When probes were added to the influent solution, the highest oxidant production occurred inside the NBOT unit. These results show that the treatment occurring inside the unit is most substantial. For most effective treatment, the highest contaminant concentration to be treated should be passed through the unit during deployment.

•OH production was highly dependent on the pH of the solution and whether O_2 or O_3 feed gas was used. During oxygen nanobubble treatment without ozone present, cumulative •OH generation was minimal and occurred only at low pH. At high pH, no measurable amount of •OH was produced inside the unit or over time in effluent solution. The lack of oxidant formation during nanobubble treatment without ozone present indicates that O_2 nanobubble treatment alone is ineffective as an advanced oxidation process.

During ozone treatment at high pH, •OH production occurred within the NBOT unit but no increase in cumulative [•OH] over time was observed. During ozone treatment at low pH, the •OH production inside the unit was ~20% of the production at high pH. However, a ~300% increase in cumulative [•OH] was observed over the first week following treatment. The cumulative [•OH] continued to increase over the course of 30 days until reaching and plateauing at the concentration observed at high pH. These results suggest that additional •OH production following initial treatment only occurs at low pH.

Immediately following treatment, $[O_3]_{aq}$ was ~80% of the cumulative concentration produced over time. The remaining 20% of the cumulative $[O_3]_{aq}$ increased during the first week following treatment, before plateauing and reaching the final cumulative concentration, which was over 500% of the cumulative [•OH]. These results suggest that most of the delivered ozone is immediately transferred to aqueous ozone at low pH.

References

1. Glaze, William & Kang, Joon-Wun & Chapin, Douglas. (1987). The Chemistry of Water Treatment Processes Involving Ozone, Hydrogen Peroxide and Ultraviolet Radiation. Ozone-science & Engineering - OZONE-SCI ENG. 9. 335-352. DOI: 10.1080/01919518708552148.
2. Attard, P. (2013). The stability of nanobubbles. The European Physical Journal Special Topics, 1-22.
3. Agarwal, A., Ng, W. J., & Liu, Y. (2011). Principle and applications of microbubble and nanobubble technology for water treatment. Chemosphere, 84(9), 1175–1180. DOI: 10.1016/j.chemosphere.2011.05.054
4. Batagoda, J. H., Hewage, S. D. A., & Meegoda, J. N. (2018). Nano-ozone bubbles for drinking water treatment. Journal of Environmental Engineering and Science, 14(2), 57-66.
5. Standard Methods Committee of the American Public Health Association, American Water Works Association, and Water Environment Federation. 4500-o3 ozone (residual) In: Standard Methods For the Examination of Water and Wastewater. Lipps WC, Baxter TE, Braun-Howland E, editors. Washington DC: APHA Press.
6. Gonzalez, David & Kuang, Xiaobi & Scott, John & Da Rocha, Gisele & Paulson, Suzanne. (2018). Terephthalate Probe for Hydroxyl Radicals: Yield of 2-Hydroxyterephthalic Acid and Transition Metal Interference. Analytical Letters. 51. 1-10. 10.1080/00032719.2018.1431246.

Concept for an Experimental Study Investigating Effects of Coriolis Forces on Cavitation-Bubble Collapse in an Ultra-High-Speed Rotating System

Peter J. Thomas[1], Iakovos Tzanakis[2], Paul Prentice[3], Marko Hočevar[4] Matvež Dular[4]

[1]*Fluid Dynamics Research Centre, School of Engineering, University of Warwick, Coventry CV4 7AL, U.K.*
[2]*School of Engineering, Computing and Mathematics, Oxford Brookes University, Oxford OX3 0BP, U.K.*
[3]*James Watt School of Engineering University of Glasgow, Glasgow G12 8QQ*
[4]*Faculty of Mechanical Engineering, University of Ljubljana, Aškerčeva cesta 6,1000 Ljubljana , 1000 Ljubljana, Slovenia*

1. Introduction

Coriolis effects, arising from background system rotation, can result in numerous, unique and often highly counter intuitive, effects on fluid flows (cf. [1]). Cavitation occurs frequently in rotary or swirling flows (e.g. ship propellers). However, due to the short time scales, and the small spatial scales, associated with cavitation-bubble dynamics, in comparison to the time scale relevant to the rotary flow, Coriolis effects are not relevant in currently existing technological contexts. Coriolis effects are not addressed in any of the textbooks on cavitation (e.g. [2-8]). Nevertheless, it is in principle possible to design a laboratory experiment where Coriolis effects should exist. We believe that these effects could, potentially, be exploited beneficially in the context of new, cavitation-based industrial technologies.

2. Objectives

The objective of the presentation is to outline the concept for the experimental configuration required to induce strong Coriolis effects on cavitation bubbles, to discuss the relevant parameters governing the process, to illustrate when Coriolis effects can be expected to affect cavitation-bubble dynamics, to speculate as regards what its effects might be and to discuss in which contexts one might, potentially, beneficially exploit the effects that arise. The long-term goal is to design, build and test a rig that enables performing experiments investigating the effects induced by Coriolis forces on cavitation bubbles under the extreme conditions at ultra-high-speed background rotation.

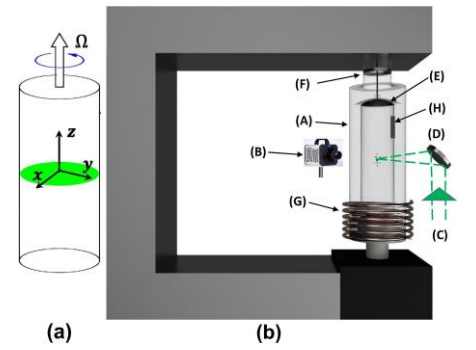

Figure 1: Concept for ultra-high-speed rotational cavitation rig. (A), Rotating container; (B), Video camera; (C), Pulsed laser; (D), Parabolic mirror; (E), Pressure sensor/reflector; (F), Power-generation unit; (G) Magnetostrictive excitation coil for generation of acoustic cavitation; (H) PVDF patch on inner wall.

3. Experimental Rig & Theoretical Considerations

The concept for the envisaged rig is illustrated in Fig. 1. The new approach is to generate cavitation bubbles within a small (height and diameter each approx. 40 mm) liquid-filled (liquid density ρ), high-speed-rotating cylindrical container. The rotational velocity, Ω (rotation frequency f), around the z axis is sufficiently high such that strong Coriolis effects will be expected. Bubbles themselves are to be generated inside the container by means of standard methodologies (laser or ultrasonic excitation).

The rotation induces a radial pressure gradient dp/dr of increasing pressure, from the axis of rotation to the inner container wall. The pressure gradient depends on the rotational velocity Ω. The cavitation bubbles will naturally be restrained to the central z-axis, due to the radial pressure gradient.

It is well known that the collapse of cavitation bubbles located in the vicinity of rigid walls creates powerful liquid jets [2-8]. For a cavitation bubble located near the top or bottom wall of the container the direction of the jet would be aligned with the z-axis (towards the wall).

The Coriolis force is given by $\overrightarrow{F_C} = -2\rho\vec{\Omega} \times \vec{U}$. Coriolis effects are expected when the Rossby number, $Ro = U/2\Omega L$ adopts values $Ro \lesssim 1$. The Rossby number characterizes the ratio of inertial and Coriolis forces. The relevant characteristic velocity scale is $U = d_c/t_c$, where d_c and t_c represent, respectively, the bubble diameter and the bubble-collapse time. The magnitude of the collapse time is of the order 10^{-4} s. The relevant characteristic length

scale L corresponds to the bubble diameter. Therefore, one finds that Coriolis forces are important when $f \geq 1/(4\pi t_c) \approx 800$ Hz, corresponding to $48{,}000$ rpm. Devices to achieve rotation rates of that magnitude, or above, are available. For instance, commercial wood routers for under €100 operate at rotation rates up to $32{,}000$ rpm and turbo charger rotate at rates of up to around $360{,}000$ rpm (see e.g. [9]). However, very challenging design issues will be associated with balancing the rig at such operational speeds and ensuring the integrity of a transparent container under these conditions.

For strong rotation (i.e. at low Rossby numbers) there exists a tendency to suppress vertical gradients $\partial/\partial z$ of the flow-velocity components u and v associated with the horizontal x and y coordinate directions in the spinning container in Fig. 1. This phenomenon is known as the Taylor-Proudman theorem. If u, v have certain values at a particular height z, say at the height of the green plane in Fig. 1(a), then these velocity values have to remain unchanged for any other position along the z-axis. That is, background rotation has a 'rigidifying' effect on the fluid and this leads to the formation of so-called Taylor columns, which are well-documented in the literature [1]. This implies, in turn, that a 3D bubble implosion should tend to align itself with the z-coordinate axis, the axis of rotation, to generate a more powerful wall-directed jet. In the planned experiments the Rossby number will be substantially below one. Thus, the Taylor-Proudman theorem indicates that significant new effects in cavitation-bubble dynamics can be created. The Coriolis induced effects will be complemented by the extremely large radial pressure gradients. For instance, we have estimated that for a small water-filled container of radius $R = 20$ mm spinning between $30{,}000 - 60{,}000$ rpm ($500 - 1000$ Hz) pressures between $20 - 80$ atm will exist at the inner container wall. That corresponds to the pressure existing at a depth of $200 - 800$ m below the surface of the ocean and the associated radial pressure gradients are of the order of $1 - 4$ atm/mm.

4. Potential Applications and Conclusion

The expectation is that the extreme conditions offer the potential to increase and focus the energy released during bubble collapse. This could be exploited for manufacturing nano-materials, food processing or pharmaceutics. To the best of our knowledge such a study has never been performed anywhere before. There exists the possibility for a quantum-leap advance of our knowledge about cavitation, leading to entirely new branches in the physics of ultrasonic cavitation processing and cavitation intensification.

References

[1] Davidson, P.A. 2013 Turbulence in rotating, stratified and electrically conducting fluids, Cambridge University Press.
[2] Brennen, E.B. 2013 Cavitation and Bubble Dynamics, Cambridge University Press.
[3] Franc, J.-P. & Michel, J.-M. (Eds.) 2005 Fundamentals of cavitation, Kluwer Academic Publishers.
[4] Washio, S. 2014 Recent developments in cavitation mechanisms: A guide for scientists and engineers, Woodhead Publishing.
[5] d'Agostino, L. & Salvetti M.V. (Eds.) 2017 Rotordynamics Effects an Turbopumps and Hydroturbines, Springer.
[6] Yasui, K. 2018 Acoustic cavitation and bubble dynamics, Springer.
[7] Wan, M., Feng, Y. & ter Haar, G. 2015 Cavitation in biomedicine, Springer.
[8] Li, S. (Ed.) 2001 Cavitation in hydraulic machinery, Imperial College Press.
[9] https://www.turbopacs.com/root-cause-analysis/over-speeding/

Tannin Extraction from Chestnut Wood Waste Using Hydrodynamic Cavitation: Preliminary Patterns and Quantitative Assessment

Francesco Meneguzzo[1,2]

[1] *Institute of Bioeconomy, National Research Council of Italy, 10 Via Madonna del Piano 10, 50019 Sesto Fiorentino (FI), Italy*
[2] *Central Scientific Committee, Italian Alpine Club, 19 Via E. Petrella, I-20124 Milano, Italy*
Email: francesco.meneguzzo@cnr.it

1. Introduction

Chestnut (*Castanea sativa* Mill.) wood waste, mostly generated by sawmill works, can be extracted in water to obtain practically only hydrolysable tannins, which are insensitive to temperature and unaffected by enzymes, offering an interesting chance to assess the feasibility, yield and economy of extraction processes using hydrodynamic cavitation (HC). Chestnut tannin (CT) is a commodity with consolidated technical uses and emerging uses in food and medicine [1,2], yet locally abundant wood waste resources are still mostly untapped. The feasibility of HC-based CT extraction over a range of solid (dry mass) to liquid ratios (SLR) was recently shown at the real scale [2]. The extraction yield and the overall efficiency of the process are affected by the biomass concentration (BC), as well as by more subtle effects related to the hydraulic circulation of fibrous wood particles with large aspect ratio, particle size and saturation, turbulence and shear. Slurries of fibrous biomass particles could dampen turbulence, lower friction and pressure losses, and increase the efficiency of centrifugal pumps over pure water only conditions [3–5].

2. Objectives

This study aimed at providing a deeper insight into the HC-based CT extraction processes, including pump's efficiency, extraction rate, process yield (PY), and overall economy.

3. Materials & methods

The chestnut wood samples, smaller than 3 mm in linear size, were extracted in tap water only at room pressure. Experimental details were described in previous study, including the HC extractor with a circular Venturi reactor [6], materials, tests identification, measurement methods and computation of the cavitation number (CN) [2]. A further test is presented here, with a substantially higher SLR of 1:6.

4. Results

Figure 1 shows absorbed power (POW), CN (water-only), and heating efficiency (HE), against process temperature. HE was computed as the percentage ratio of the heat supplied to the water-wood mixture to the consumed electricity, accounting for both pump's efficiency and thermal dissipation.

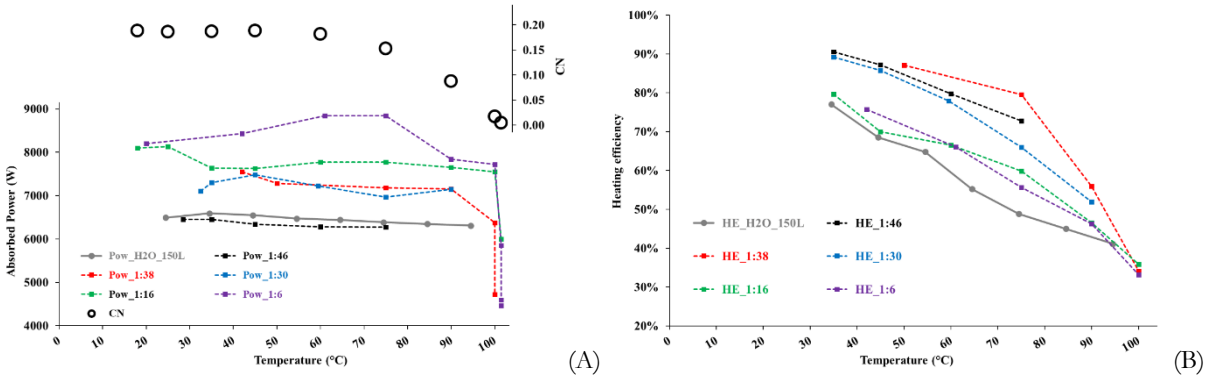

Figure 1: (A) Absorbed power and CN; (B) Heating efficiency.

POW grew non-linearly with BC, exceeding the water-only condition at SRL greater than 1:46, and collapsing at temperatures above 90°C. CN was fairly constant at the level of 0.18 until 60°C, then decreased down to 0.09 at 90°C and 0.02 at 100°C, with supercavitation starting between 90°C and 100°C. Despite higher power consumption, HE was always substantially greater than with pure water only (e.g., at 60°C, water-only HE was 50%, and with SRL of 1:38 was greater than 80%), and generally decreased non-linearly

with BC. Likely, the HC-driven fast grinding and microporosity enhancement of the wood particles, and the enhancement of mass transfer leading to fast biomass saturation, contributed to the drag reduction and the increase in pump's efficiency. The HE collapse above 75°C was likely due to increased thermal friction and heat dissipation, and eventually by supercavitation. Further investigation is recommended.
CT extraction rate is known to increase with water temperature, and the microporosity enhancement during developed cavitation likely boosted the later extraction rate [2]. Thus, the high HE favorably affected PY. Figure 2 shows the cumulative CT extraction rate over time, and the same quantity, along with the specific energy (energy consumed per unit mass of extracted CT), against temperature.

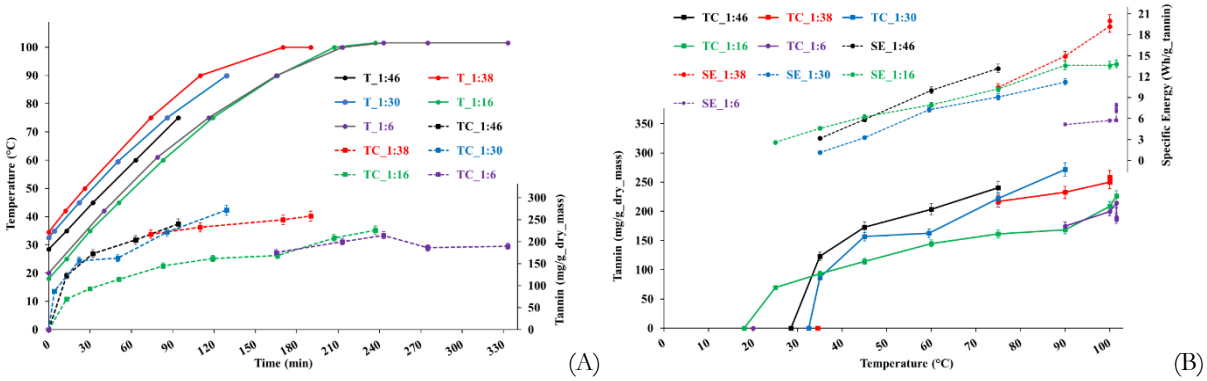

Figure 2: (A) Cumulative CT extraction rate over time; (B) Cumulative CT extraction rate and specific energy against temperature.

CT extraction rate per unit dry biomass showed two distinct patterns: higher levels at low BC, up to 1:30, and lower levels at higher BC, with the frequency of cavitation events hitting single particles likely playing a role, however in a remarkable non-linear way. A process time of 30 minutes at boiling point provided the highest rate in the highest BC test (1:6), which showed also by far the highest PY (inverse of the specific energy). Interestingly, test 1:30 showed higher PY than test 1:16, likely due to substantially higher HE levels.

5. Conclusions

CT extraction using HC was technically feasible, revealed a few interesting points, and left ample room for further improvement. At the optimal conditions found so far, i.e., BC of 1:6, 30 minutes at boiling point, with specific energy consumption of 5.7 Wh per g of extracted CT, and assuming a power price of 0.45 €/kWh, the specific operational production cost of CT would be about 2.6 €/kg. Including the further steps of pre-grinding (or sieving), separation, concentration and spray-drying, the total manufacturing cost of dry CT was estimated around 5 €/kg.
Further process optimization might include, among the other things: further increasing HE at high BC conditions; increasing cavitational yield (higher bubble density); experimenting at higher BC.

References

1. Pagliaro t al. Tannin: A New Insight into a Key Product for the Bioeconomy in Forest Regions. *Biofuels, Bioproducts and Biorefining* **2021**, doi:10.1002/bbb.2217.
2. Meneguzzo et al. Pilot Scale Tannin Extraction from Chestnut Wood Waste Using Hydrodynamic Cavitation. In Proceedings of the Towards a Smart, Resilient and Sustainable Industry. ISIEA 2023. Lecture Notes in Networks and Systems, vol 745; Borgianni, Y., Matt, D.T., Molinaro, M., Orzes, G., Eds.; Springer, Cham, **2023**; pp. 437–447; doi:10.1007/978-3-031-38274-1_36.
3. Vaezi et al. Investigation into the Mechanisms of Pipeline Transport of Slurries of Wheat Straw and Corn Stover to Supply a Bio-Refinery. *Biosyst Eng* **2014**, *118*, 52–67, doi:10.1016/j.biosystemseng.2013.11.006.
4. Luk et al. Pipeline Transport of Biomass: Experimental Development of Wheat Straw Slurry Pressure Loss Gradients. *Biomass Bioenergy* **2014**, *64*, 329–336, doi:10.1016/j.biombioe.2014.03.046.
5. Vaezi et al. The Flow of Wheat Straw Suspensions in an Open-Impeller Centrifugal Pump. *Biomass Bioenergy* **2014**, *69*, 106–123, doi:10.1016/j.biombioe.2014.07.009.
6. Meneguzzo et al. Real-Scale Integral Valorization of Waste Orange Peel via Hydrodynamic Cavitation. *Processes* **2019**, *7*, 581, doi:10.3390/pr7090581.

Cavitation alone or in combination with plasma for waterborne virus inactivation

Arijana Filipić[1], David Dobnik[1], Maja Ravnikar[1], Tamara Košir[1], Martin Petkovšek[2], Mojca Zupanc[2], Jure Zevnik[2], Jernej Oratar[2], Matevž Dular[2], Miran Mozetič[3], Rok Zaplotnik[3], Gregor Primc[3], Ion Gutiérrez-Aguirre[1]

[1]*National Institute of Biology, Ljubljana, Slovenia*
[2]*University of Ljubljana, Faculty of Mechanical Engineering, Ljubljana, Slovenia*
[3]*Jožef Stefan Institute, Ljubljana, Slovenia*

1. Introduction

Microbially polluted water can contain various pathogens, including viruses, and is a source for the spread of various diseases. For instance, waterborne human enteric viruses infect millions of people each year, leading to increased hospitalization rates and mortality. In addition, waterborne plant viruses can destroy crops, leading to financial losses and food shortages. This becomes even more relevant with the global increase of arid regions, where reuse of wastewater in irrigation is becoming an alternative to water scarcity. This is why the use of technologies that can efficiently inactivate viruses is so important.
In recent years, several environmentally friendly methods for water decontamination have emerged. Two of these methods are hydrodynamic cavitation and non-equilibrium/cold plasma. When hydrodynamic cavitation bubbles collapse, extreme mechanical effects (e.g., extreme shear forces, shock waves, pressure pulsations, high temperatures, and microjets) are generated in their microenvironment, which can also lead to the formation of OH and H radicals. Both mechanical effects and radicals can inactivate viruses by disrupting their integrity and by oxidation, respectively. During plasma treatment, various short- and long-lived reactive species are formed, depending on various factors such as the type of sample treated and the gas. These species can also inactivate viruses by oxidation. In addition, plasma emits ultraviolet and/or vacuum ultraviolet photons that can affect viral nucleic acids and thus prevent viral replication. However, it is challenging to introduce gaseous plasma into the liquid. Therefore, coupling with another method that enables gas in a liquid, such as cavitation, could solve this challenge.

2. Objectives

In the first part of our studies, our aim was to evaluate the efficiency of hydrodynamic cavitation in inactivating various viruses in water. In the second part, the main objective was to construct a unique device combining supercavitation with plasma and test its inactivation potential.

3. Materials & methods

In the first part of the studies, we used a hydrodynamic cavitation test rig with the Venturi constriction (Figure 1) to treat viruses in water, e.g., potato virus Y (PVY) and bacteriophage phi6. We treated PVY, an important plant pathogen that can cause high losses in potato crops, with initial concentrations of 10^5 to 10^6 RNA copies/µL of the sample. Furthermore, in light of the COVID-19 pandemic, we also treated bacteriophage phi6, which is often used as a surrogate of SARS-CoV-2. We worked with initial concentrations of 10^6 to 10^7 plaque-forming units (PFU)/mL. In all experiments, we treated 1 L of water that was pushed from one reservoir to another by pressurized air. In each pass, the sample passed through the constriction where it was cavitated. The pressure difference between the two reservoirs was maintained at 7 bar. Inactivation efficiency was determined using test plant infectivity assays for PVY and plaque assays for phi6.

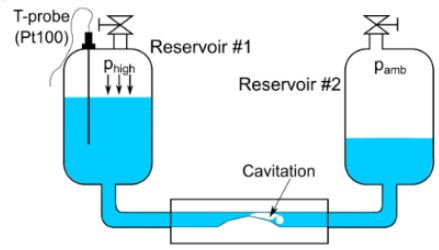

Figure 1: Schematic representation of hydrodynamic cavitation test rig [1]

In the second part of our studies, we constructed a device combining supercavitation with non-equilibrium plasma (Figure 2). After optimizing the device, we performed several experiments. We treated ~0.5 L of circulating water with bacteriophage MS2, a surrogate of human enteric viruses at a concentration of 10^5 to 10^6 plaque-forming units/mL. We determined the efficiency of virus inactivation using infectivity plaque assay.

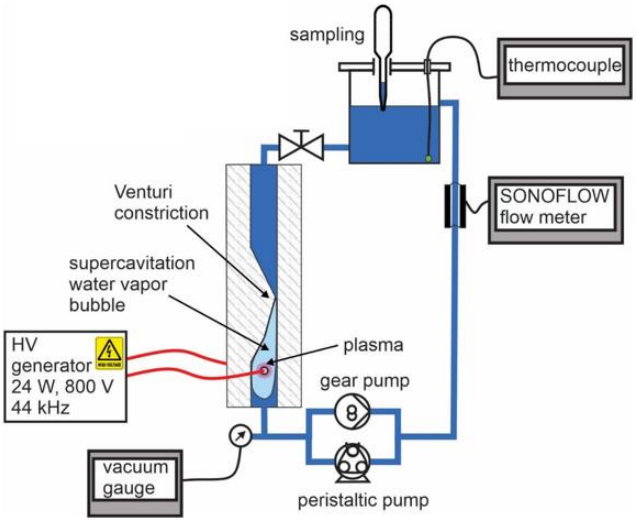

Figure 2: The schematic of the combined plasma-supercavitation device (not to scale). Pressure, water flow, temperature, pH, and H_2O_2 production were monitored during the experiments[2].

4. Results

We successfully inactivated PVY with hydrodynamic cavitation after 500 passes (lasting about 50 minutes) in all experiments, whereas even shorter treatments of 125 or 250 passes were sufficient in some experiments[1]. Inactivation of phi6 was time- and temperature-dependent, with longer treatments and higher temperatures providing the best inactivation. For example, at water temperatures of 10 and 20 °C, inactivation occurred after 1000 passes predominantly by the mechanical effect of cavitation and resulted in a reduction of up to 4.5 logs, whereas at 30 °C the reduction increased to up to 6 logs and was strongly influenced by the elevated temperature, which likely made the virus more sensitive to the cavitation treatment[3].

Inactivation of bacteriophage MS2 with the combined supercavitation and non-equilibrium plasma technology was also time-dependent, with better inactivation achieved with longer treatments. Inactivation of more than 5 logs was achieved after only 4 min of treatment[2].

5. Conclusions

Hydrodynamic cavitation can successfully inactivate different types of viruses in water. However, rather long treatment times are required to achieve high inactivation. On the other hand, the combination of supercavitation with non-equilibrium plasma provided fast virus inactivation, suggesting that this technology could be used for decontamination of various water sources.

References

1. Filipić, A. *et al. Hydrodynamic cavitation efficiently inactivates potato virus Y in water. Ultrasonics Sonochemistry* vol. 82 (2022).

2. Filipić, A. *et al.* Cold plasma within a stable supercavitation bubble - a breakthrough technology for efficient inactivation of viruses in water. *In Review* (2023).

3. Zupanc, M. *et al.* Inactivation of the enveloped virus phi6 with hydrodynamic cavitation. *Ultrason Sonochem* **95**, (2023).

Device for water disinfection based on cavitation and cold plasma discharge

Pavel Rudolf[1], Pavel Sťahel[2], Blahoslav Maršálek[3], Jan Čech[2], František Pochylý[1], Lubomír Prokeš[2], Eliška Maršálková[3], Marek Balko[1]

1Brno University of Technology, Faculty of Mechanical Engineering, V. Kaplan Department of Fluid Engineering
[2]Masaryk University, Faculty of Science, Department of Physical Electronics
[3]Czech Academy of Sciences, Botany Institute

1. Introduction

Wastewater treatment becomes of utmost importance with increasing water resources scarcity. It becomes even more important with growing pollution in form of so called micropollutants (residuals of pharmaceuticals, pesticides, hormones, personal care products and other persistent organic compounds). Situation is reflected also in EU legislation and new Water framework directive tackles the issue of micropollutants removal in the last stage of wastewater treatment process.

2. Advanced oxidation processes (AOP) based on hydrodynamic cavitation (HC)

AOPs are one of technologies that can be utilized for micropollutants elimination (UV, ozonization, peroxidation, etc.). Some of them are based or can be combined with hydrodynamic cavitation. While using pure hydrodynamic cavitation is promising for mitigation of biological contamination [1], it is not so successful and efficient for chemical compounds, including cyanobacteria toxins. Then different combinations of HC and other AOPs provide a significantly improved performance [2, 3].
Plasma technologies for water treatment are also AOP, but until recently their application was limited to laboratory scale [4]. Approaches applied for plasma treatment are: plasma generated over the surface, plasma generated within gas bubbles, diaphragm discharge. None of them enables large volume treatment relevant for practical applications.

3. CaviPlasma®

New approach based on synergy of hydrodynamic cavitation and cold plasma discharge was invented and patented [5-7], which couples both effects together. Hydrodynamic cavitation creates a vapor bubble cloud, which is a gaseous environment favourable for plasma discharge, low pressure allows for extension of discharge length compared to atmospheric pressure and of course HC is also important for bringing high mechanical stresses and increased mixing. Result of the plasma discharge is a strong electrical field, where water molecules dissociate, hydroxyl radicals arise and later recombine into hydrogen peroxide. Both hydroxyl radicals and hydrogen peroxide are strongly oxidative. On top ozone is formed and UV light irradiated, further enhancing elimination efficiency of CaviPlasma. CaviPlasma allows treatment of large volumes of water. Even smaller laboratory unit works with flow rate of 1 m^3/hour, bigger unit with 15 m^3/hour.
HC is formed in a Venturi tube, electrical part consists of high voltage electrode and grounded electrode. High voltage custom made generator based on low voltage tunable generator and high voltage transformer is attached to high voltage electrode.

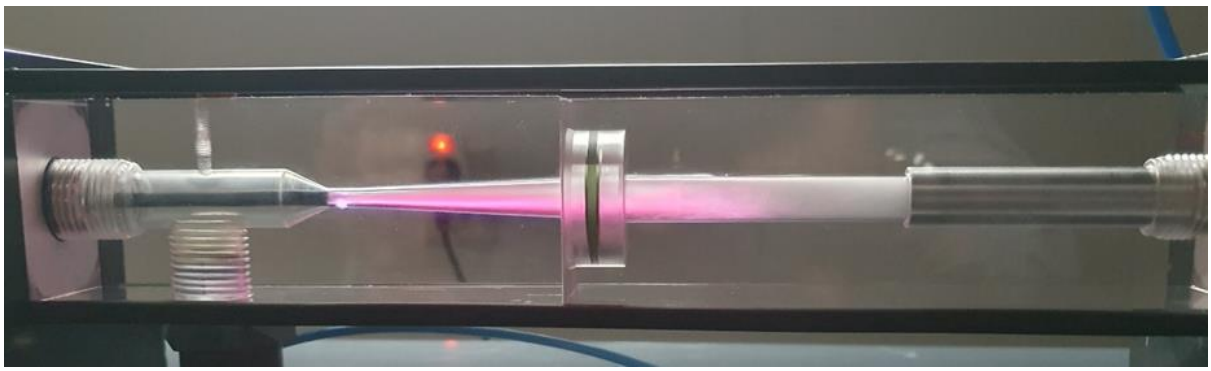

Figure 1: CaviPlasma device

4. Results

CaviPlasma is producing around 10 mg of hydrogen peroxide per one pass and its production efficiency is 9 g of hydrogen peroxide per kWh. Energy efficiency is around 1 kWh per one cubic meter of the treated water.

Application on cyanobacteria proved their inactivation even in a single pass [8], elimination of pharmaceutical residuals from water proved more than 90% efficiency (for some contaminants even higher).

5. Conclusions

CaviPlasma is a promising AOP technology aiming on the last stage of wastewater treatment for micropollutant removal. Moreover CaviPlasma can also produce from tap water so called plasma activated water (PAW) [9] with high content of stable hydrogen peroxide, which can be further used in agriculture to fight fungal or bacterial diseases of plants or fish, for surface disinfection in hospitals or decontamination in case of handling water contaminated by cyanobacteria toxins.

References

[1] Dular et al: Use of hydrodynamic cavitation in (waste)water treatment, Ultrason Sonochem, 29, 2016

[2] Marsalek et al: Synergistic effects of trace concentrations of hydrogen peroxide used in a novel hydrodynamic cavitation device allows for selective removal of cyanobacteria, Chem.Eng.J., 2020

[3] Zezulka et al: High-pressure jet-induced hydrodynamic cavitation as a pre-treatment step for avoiding cyanobacterial contamination during water purification, J.Env.Manag., 2020

[4] Takeuchi, N., Yasuoka, K.: Review of plasma-based water treatment technologies for the decomposition of persistent organic compounds, Jpn. J. Appl. Phys. 60 SA0801, 2021

[5] Rudolf, P.; Pochylý, F.; Sťahel, P.; Ráheľ, J.; Čech, J.; Maršálek, B. Apparatus for purifying liquids and a method for purifying liquids using this apparatus. Czech Patent No. 308532, 13.12.2019

[6] Rudolf, P.; Pochylý, F.; Sťahel, P.; Ráheľ, J.; Čech, J.; Maršálek, B. PCT/CZ2020/000054, international patent application (2020)

[7] Rudolf, P.; Pochylý, F.; Sťahel, P.; Ráheľ, J.; Čech, J.; Maršálek, B. Israel patent 293579, Device for treatment of liquids and the method of treatment of liquids with use of this device, 2.8.2023

[8] Maršálek, B.; Maršálková, E.; Odehnalová, K.; Pochylý, F.; Rudolf, P.; Stahel, P.; Rahel, J.; Čech, J.; Fialová, S.; Zezulka, Š. Removal of *Microcystis aeruginosa* through the Combined Effect of Plasma Discharge and Hydrodynamic Cavitation.*Water* 2020, *12*, 8

[9] Čech, J.; Sťahel, P.; Ráheľ, J.; Prokeš, L.; Rudolf, P.; Maršálková, E.; Maršálek, B. Mass Production of Plasma Activated Water: Case Studies of Its Biocidal Effect on Algae and Cyanobacteria. *Water* 2020, *12*, 3167

Acknowledgement

Czech Science Foundation is acknowledged for support of the research under project 22-11456S "Exploring fundamental interactions of hydrodynamic cavitation and low-temperature plasma to enhance the disinfection effects".

Water droplet impact on thin liquid crystal films

Uroš Tkalec[1,2,3], Rok Štanc[1], Yang Xu[4], Robert Dupont[4], Xiaoguang Wang[4,5]

[1]*Institute of Biophysics, Faculty of Medicine, University of Ljubljana, Slovenia*
[2]*Faculty of Natural Sciences and Mathematics, University of Maribor, Slovenia*
[3]*Department of Condensed Matter Physics, Jožef Stefan Institute, Slovenia*
[4]*Department of Chemical and Biomolecular Engineering, The Ohio State University, Ohio, U.S.A.*
[5]*Sustainability Institute, The Ohio State University, Ohio, U.S.A.*

1. Introduction

Understanding of droplet impact on solid or liquid surfaces is essential for a variety of practical applications such as combustion, self-cleaning, inkjet printing, agricultural sprays, anti-icing, and the pharmaceutical and food industries [1]. To date, extensive studies have reported droplet dynamics on two types of bioinspired slippery surfaces [2]. The first type of superhydrophobic surfaces with hierarchical topography can often completely bounce droplets due to the presence of air pockets, but these can collapse under high pressure. To address the vulnerability of superhydrophobic surfaces, pitcher plants have inspired researchers to develop slippery lubricant-infused porous surfaces, namely SLIPS [3]. Although the effects of Weber number, thickness, and viscosity of lubricating films on droplet bouncing have been extensively studied [4], SLIPS currently rely exclusively on isotropic lubricants such as silicone and fluorinated oils [5], which inherently lack long-range positional and orientational order of their constituent molecules. The role of molecular order in structured fluids for droplet impact dynamics and bouncing is therefore still largely unknown.

2. Objectives

We study the effects of water droplet impact on a representative class of anisotropic structured fluids called thermotropic liquid crystals (LCs). These combine properties commonly associated with crystalline solids (long-range molecular order) and isotropic liquids (high molecular mobility). LCs exhibit a rich pattern of mesophases with an intrinsic positional and orientational ordering of rod-shaped molecules that have enabled a wide range of functional surfaces capable of directed assembly of molecules and particles, liquid transport, and activated release of chemicals encapsulated within their bulk [6, 7]. Although LCs can offer unprecedented complexity compared to isotropic oil-based SLIPS, the water droplet-induced dewetting of LC films coated on conventional hydrophobically modified substrates has largely precluded the exploration of the role of molecular orders in different LC mesophases on droplet impact at LC interfaces. In this work, we use the pitcher plant strategy to design and fabricate LC-infused porous surfaces (LCIPS) against dewetting by water droplets [8], which allow us to study droplet behavior (e.g., sliding, spreading, receding, and bouncing) at different Weber numbers. In particular, we show that the temperature-dependent LC mesophases have little effect on spreading behavior, but significantly change the retraction rate of the impinging droplets. Thin LC films generally prevent rebound, so we focus mainly on phenomena of the deposition regime. Finally, we investigate the effects of LC mesophase on cargo transport across water-LC interfaces after water droplets impinge on a thin LC film.

3. Materials & methods

We use 8CB LC, to impregnate LCIPS and form about 100 micrometers thick film; design and synthesis of LCIPS are described in [8]. Deionized water droplets with a diameter of 2 to 3 mm are generated by means of the pendant method. The drop impact dynamics is observed using a high-speed camera with a 1x microscope objective at 10000 frames per second, which allows capturing the fast dynamics of the droplet at the impact and its evolution. LED panels are placed behind the sample to provide a sufficient illumination for the experiments. The collected videos are analyzed using a custom-made procedure in Python and ImageJ software. Some LCIPS samples were loaded with aqueous ethyl orange labeled microdroplets to study cargo transfer across water-LC interfaces, and some water droplets were loaded with SDS stabilized oil blue labeled 8CB microdroplets for the same purpose. The Weber number was varied between 20 and 200. The schematic representation of the experiment is shown in Fig. 1.

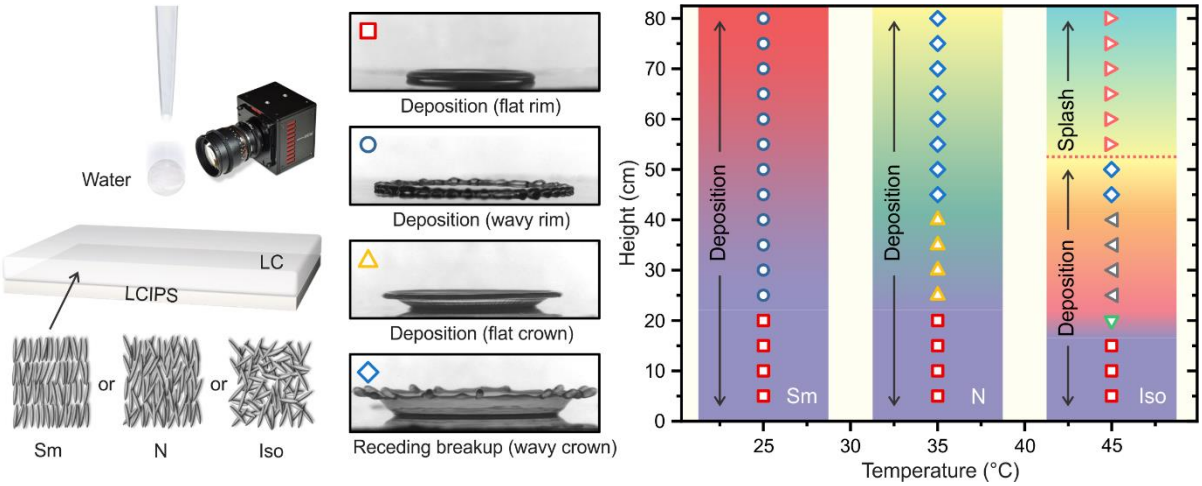

Figure 1: Schematic diagram of the experiment (left) showing the impact of a drop of water on a thin LC film of a particular mesophase. Some possible outcomes are shown in the middle, while an overview of the droplet impact phenomena is given on the right.

4. Results

We analyze how the LC film thickness, surface tension, dynamic viscosity, and molecular order in smectic (Sm), nematic (N), and isotropic (Iso) mesophases determine the outcomes of droplet impact phenomena. The post-impact dynamics are characterized as a function of Weber number, Reynolds number, retraction velocity, and the formation of wrapping layer. Furthermore, we demonstrate that the intrinsic molecular order of LCs can selectively trigger mass transport across the water-LC interfaces at a given Weber number. By tuning the LC mesophases and droplet impact dynamics, we can achieve different regimes, including no cargo transfer, unidirectional transfer, and even bidirectional transfer.

5. Conclusions

Our results reveal that the characteristic positional and orientational order of LC mesogens can significantly affect droplet impact behavior and micro-cargo release. Since the mesophases of LCs can be reversibly switched by a wide range of external stimuli, the results of this work open up a new and versatile class of stimuli-responsive surfaces that can control mass transfer processes that have the potential for smart manufacturing such as drop impact printing of highly viscous fluids.

References

[1] A. L. Yarin, Drop impact dynamics: splashing, spreading, receding, bouncing… *Annu. Rev. Fluid Mech.* **38**, 159-192 (2006).
[2] Y. Liu, X. Yan, Z. Wang, Droplet dynamics on slippery surfaces: small droplet, big impact. *Biosurf. Biotribol.* **5**, 35-45 (2019).
[3] T. S. Wong, S. H. Kang, S. K. Tang, E. J. Smythe, B. D. Hatton, A. Grinthal, J. Aizenberg, Bioinspired self-repairing slippery surfaces with pressure-stable omniphobicity. *Nature* **477**, 443-447 (2011).
[4] M. Muschi, B. Brudieu, J. Teisseire, A. Sauret, Drop impact dynamics on slippery liquid-infused porous surfaces: Influence of oil thickness. *Soft Matter* **14**, 1100-1107 (2018).
[5] J. Li, E. Ueda, D. Paulssen, P. A. Levkin, Slippery lubricant-infused surfaces: properties and emerging applications. *Adv. Funct. Mater.* **29**, 1802317 (2019).
[6] E. Bukusoglu, M. Bedolla Pantoja, P. C. Mushenheim, X. Wang, N. L. Abbott, Design of responsive and active (soft) materials using liquid crystals. *Annu. Rev. Chem. Biomol. Eng.* **7**, 163-196 (2016).
[7] Y.-K. Kim, X. Wang, P. Mondkar, E. Bukusoglu, N. L. Abbott, Self-reporting and self-regulating liquid crystals. *Nature* **557**, 539-544 (2018).
[8] Y. Xu, A. M. Rather, Y. Yao, J.Fang, R. S. Mamtani, R. K. A. Bennett, R. G. Atta, S. Adera, U Tkalec, X. Wang, Liquid crystal-based open surface microfluidics manipulate liquid mobility and chemical composition on demand. *Sci. Adv.* **7**, eabi7607 (2021).

Piezocatalysys from ultrasonic irradiation of simple inorganic salts

[1]A. Troia, [2]V. Maurino, [2]F. Pellegrino, [3]S. Hernandez

[1]INRIM, Advanced Metrology for Quality of Life , Turin, Italy.
[2] Department of Chemistry UNITO, Turin, Italy
[3] Department of Applied Science and Technology, Polytechnic of Turin, Italy.

1. Introduction

The use of piezoelectric nano-microparticles exposed to ultrasonic irradiation has emerged over last 10 year as potential new application of sonochemistry in several research fields as energy, environmental up to health applications. As a consequence of ultrasonic vibrations and mechanical effect of acoustic cavitation typical of low frequency (20-60 kHz), the particles can be activated in order to promote or enhance formation of radicals, water splitting effect and different radical reactions a relatively huge number of materials have been tested piezoceramics, oxides, plastics and composite using metallic nanoparticles. The dimension and shape of the particles has a great influence on the phenomenon however, depending also of ultrasonic frequency, the theory describing the activation mechanism is not still clear [1,2,3].

2. Objectives

Here we report experimental results using simple inorganic piezoelectric or paraelectric salt as Potassium sodium tartrate tetrahydrate (Rochelle salt) and potassium dihydrogenphosphate (KH_2PO_4). Different dyes degradation experiment have been performed under ultrasonic irradiation of concentrated salts solutions. The degradation efficiency as function of salts concentration and influence of saturating gas have been investigated.

3. Materials & methods

Low frequency ultrasonic horn (Badelin HD 2200) have been used for the experiments (Figure 1). UV-vis absorbance measurements have been performed on small aliquots of treated solutions using a Nicolet GENESYS 50 UV-vis spectrometer. GC measurements have been conducted under Argon or nitrogen saturated solutions collecting the upper gas volume every 5 min of continuous sonication. For EPR spectroscopy measurements small samples of 4 ml containing DMPO trap and have been sonicated for 10 min in a small ultrasonic bath and then analyzed with Bruker EMXNanoX-Band

Figure 1: ultrasonic set-up for GC measurements

4. Results

On Figure 2 the degradation efficiency for MB in presence of Potassium sodium tartrate tetrahydrate as function of time. Surprisingly when using Rochelle salt the solution return blue after several hours standing at air, which indicate that instead of radicals degradation of BM a reduction of the dye occur. This hypothesis was confirmed by further investigation using Resazurin dye and finally verified by GC measurements which revealed the formation of H_2 molecules. On the other hand using KH_2PO_4

permanent degradation of MB was obtained but any no increase of H_2 was detected. EPR measurements revealed the presence OH radicals but with similar amount detected in pure water

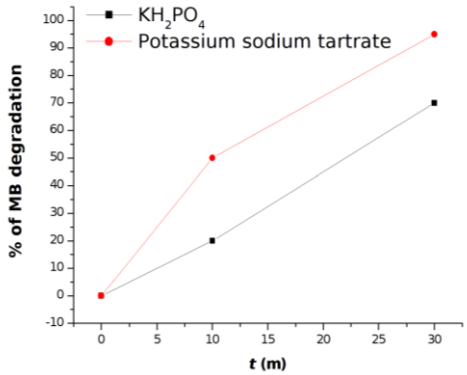

Figure 1: UV vis degradation of MB for different salts at 20 kHz

5. Conclusions

Ultrasonic irradiation of homogenous concentrated salts solutions of piezoelectric and paraelectric salts have revealed that different radicals or reduction species can be generated. The formation of reducing species using Potassium sodium tartrate could be ascribed to decarboxylation reaction activated by ultrasound and no OH radical have been detected in this case. These founding have been observed for the first time as one of the possible homogenous sonochemical reactions in aqueous solutions.

References

[1] F. Bößl et al. *Piezocatalytic degradation of pollutants in water: Importance of catalyst size, poling and excitation mode* Chemical Engineering Journal Advances 7 (2021) 100133

[2] K. Wang et al. *The Mechanism of Piezocatalysis: Energy Band Theory or Screening Charge Effect?* Angew. Chem., 134, (2022) 202110429

[3] F. Bößl et al. *Piezocatalysis: Can catalysts really dance?* Current Opinion in Green and Sustainable Chemistry 2021, 32:100537

High frequency ultrasonic water stream for cleaning processes

Takaomi Kobayashi, Orakanya Charoenvai

[1]*Nagaoka University of Technology, 1603-1 Kamitomioka, Nagaoka, Japan 940-2188*

1. Introduction

Ultrasound-based method is an effective cleaning technique for a variety of surfaces, extensively applied in several fields. In general, cleaning products such as hand soap are widely used to clean hands. These products are chemically composed of surfactants, acid or alkali, and solvents for disinfection [1]. These chemicals may cause allergy and other side effects on the skin and environment. Unlike chemical method, ultrasonic cleaning is the process that used ultrasound (US) to create cavitation bubbles in aqueous fluids, which have the cleaning effect [2]. Among the various ultrasonic devices are those that flush and clean with ultrasonic water [3]. However, there have been few studies on cleaning using ultrasonic water streams, and the situation is not well understood. This study examines its cleaning effectiveness.

2. Objectives

The present research aims to study cleaning process on surface and disinfection process that simple, cheap, effective, and chemical-free as used with ultrasonic water stream. The surfaces containing ink or contaminated with Escherichia coli (E. coli) were washed through flowing ultrasonic water stream generated at 430 kHz. The cleaning efficiency/disinfection under various conditions was evaluated detachment of ink layer from the surface and also assessed in terms of colony plate count method and survival test for E. coli in the point of view of antibacterial activity.

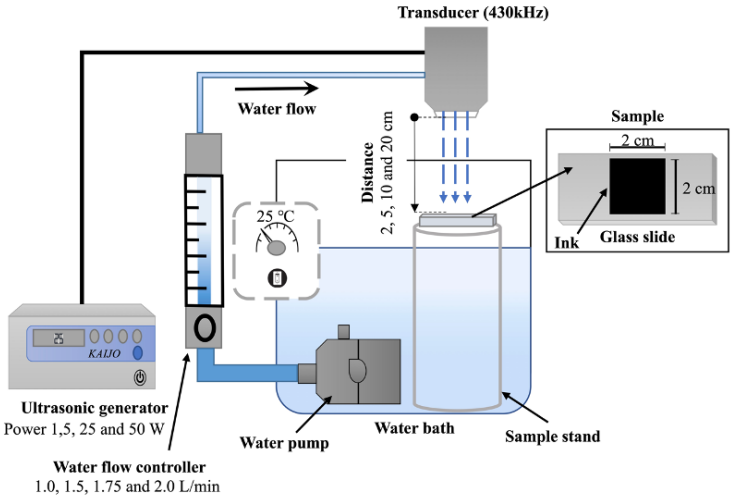

Fig. 1 Experiment setup for ultrasonic cleaning based on water stream flowing through a transducer (430 kHz) equipped with water shower nozzle

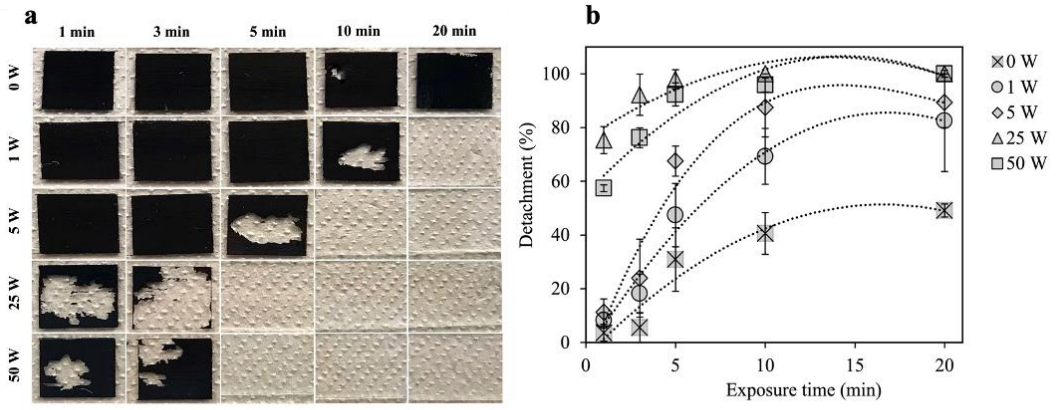

Fig. 2 Photos of samples (a) and detachment efficiency of permanent ink (b) after exposure to various ultrasonic powers and durations in water stream medium at flow rates of 1.5 L/min and and nozzle- sample distance of 5 cm.

3. Materials & methods

For cleaning surfaces contaminated with ink or E. coli, the experiment apparatus was set as shown in Fig.1. A transducer equipped with water shower nozzle was connected to the US generator (Kaijo Quava megasonic cleaner QT-003, Japan) to generate 430 kHz US waves. Tap water (5L) controlled the temperature at 30°C was circulated at the constant rate of 1.5 L/min. The water was flowed through

transducer nozzle that connected with the US device and operated at power output of 0, 1, 25, and 50 W. The distance between the nozzle and the E. coli petri dish sample was set at 5 cm. The US water was flowed through the sample for 60 seconds. The cleaning efficiencies were evaluated by measuring the detachment ink or residual colony counting. The cleaning efficiencies were evaluated by residual colony counting. One colony remaining on the dish was further grown on 90 mm plastic petri dish for survival test at 30°C for 24h.

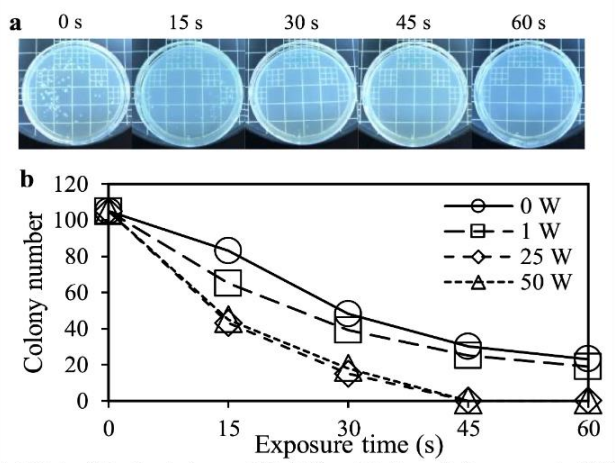

Fig.3 Photo of E. coli colonies on solidified LB media before and after exposure to 50 W US water (a) and (b) colony number of E. coli in a function of exposure time at different US powers.

4. Results

4.1. Detachment ink layer using ultrasonic water stream. In Fig. 2, pictures of the ink surface on glass slide (a) and % detachment of the ink layer (b) are shown, when the US water stream was operated at various US powers of 1, 5, 25 and 50 W for 20 min interval. The US water stream, having an 8 mm diameter, was exposed to the center of the glass surface with water flow rate and nozzle-sample distance at 1.5 L/min and 5 cm, respectively. From images shown in Fig. 2 (a), the painted glass surface after washing without US (0 W) was nearly unchanged during 5 min and a minor detachment was noticed at 10 and 20 min. This confirmed that water stream (1.5 L/min) flowing from 5 cm gap to the surface was not sufficient to remove such permanent ink. When the samples were exposed to US water stream by changing US power to 1 and 5 W, similar results were observed, but the detachment of the ink layer tended to increase at a US output power of 25 W. Quantification of the detachment (Fig. 2b) indicated that the detachment reached ≥80 % at output powers of 25 and 50 W after exposure longer than 5 min. Even though the US power was 1 W, the detachment efficiency was in the rage of 50-70%.

4.2. Disinfection of E. coli using ultrasonic water stream. Fig.3 shows residual E. coli colony number after exposure to US at power of 0, 1, 25, and 50W. It was found that the colony number on surface sample was decreased, when exposure time was increased, even though there was no US. This meant that flowing water influenced E. coli colony leach-out. % of colonies, while it was reduced to about 65 % after exposure to 1 W US. This suggested that in the presence of US power, a larger number of colonies was leached out under same water flow rate. At higher US power of 25 and 50 W, approximately 45 % of the initial colony was remained after 15 s. These powers showed high efficiency to completely remove all the colonies adhered on the sample within 45s. Then, the survival test showed that the growth tendency of E. coli was decreased as a function of exposure time. This indicated that although the colonies remained after exposure to US water, there was the lower change to grow further as compared to the normal water (0W).

5. Conclusions

It was found that ultrasonic water stream cleaning was effective in ink detachment and E. coli anti-microbial resistance without the use of soap. In both cases, the ultrasonic outputs of 25W and 50W were effective after at least 5 minutes of treatment. In particular, in the case of the E. coli survival test, no growth of bacteria was observed after 45 minutes or longer of washing, but within that time, growth of bacteria was observed even after complete washing as shown in Fig. 3. Using KI method, OH radical measurements and acoustic pressure observations indicated that the latter was effectively working for cleaning with ultrasonic water streaming.

References

[1] C. Nitsch, H.-J. Heitland, H. Marsen, H.-J. Schlüussle, Cleansing Agents,Ullmann's Encyclopedia of Industrial Chemistry (2005). Weinheim: Wiley-VCH. doi:10.1002/14356007.a07_137.

[2] N. Vyas, K. Manmi, Q. Wang, A.J. Jadhav, M. Barigou, R.L. Sammons, S.A. Kuehne, A.D. Walmsley, Which Parameters Affect Biofilm Removal with Acoustic Cavitation? A Review, Ultrasound in Medicine and Biology 45(5) (2019) 1044-1055.

[3] T.J. Bulat, Macrosonics in industry: 3. Ultrasonic cleaning, Ultrasonics 12(2) (1974) 59-68.

The abstracts should be submitted via email to matevz.dular@fs.uni.lj.si and ziga.gruden@fs.uni-lj.si until August 31st at the latest.
The abstract should no exceed 2 pages. No full paper will be required for the meeting.

Surface nano-engraving tool using shaped laser-induced cavitation

Hendrik Reese*[1], Ulisses Gutiérrez-Hernández[2], Pedro Quinto-Su[2], and Claus-Dieter Ohl[1]

[1]*Soft Matter, Institute for Physics, Otto-von-Guericke-Universität Magdeburg, Germany*
[2]*Instituto de Ciencias Nucleares, Universidad Nacional Autónoma de México*
**e-mail: hendrik.reese@ovgu.de*

1. Introduction

In our previous work [1] we showed that ring-shaped laser-induced cavitation between two glass plates, which emit a converging shock and surface wave, can be used to create surface damage at the center of the ring. By varying the time delay between the creation of two concentric ring-shaped excitations we also reported that, when both Rayleigh waves arrive at the center simultaneously, a smaller number of shots was required to produce damage, suggesting that the Rayleigh waves have a greater effect on damage generation than the shock waves.

2. Objectives

In the presented work [2] we aim to improve control of the shape of the created surface damage by varying the shape and position of the laser beam using a spatial light modulator (SLM).

3. Materials & methods

A layer of liquid (printer ink, magenta) of 80 µm height is sandwiched between two borosilicate glass plates (see figure 1A). A laser pulse (6 ns, λ = 532 nm), is focused in the liquid. To attain an elliptical laser focus, the beam is shaped by a SLM. The same configuration is modelled in three dimensions by a finite volume fluid-structure interaction simulation using OpenFOAM, where two compressible fluids are coupled to a linear elastic solid. From the laser pulse, a shock wave is launched in the liquid and a Rayleigh wave in the glass, inducing large stresses at the center of the ellipse and causing surface damage in the form of nano-sized cracks (micro-sized in length, nano-sized in depth).

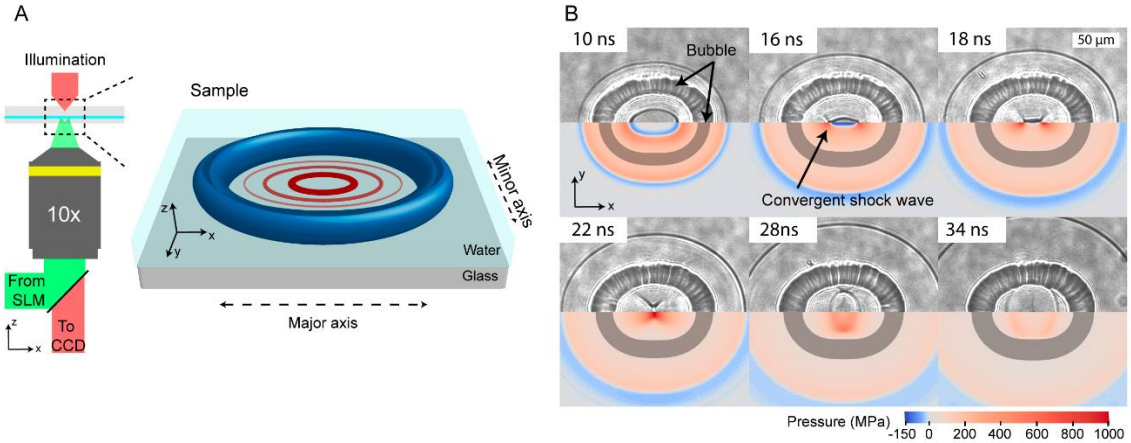

Figure 1: A Elliptical ring energy deposition with a major semi-axis of 104 µm and a minor semi-axis of 78 µm is initiated in a liquid layer of 80 µm thickness between two borosilicate glass plates. B Waves emitted by the created cavitation bubble, comparison between the experiment (top) and the simulation (bottom).

4. Results

After successive shots at the same position, a single straight crack is observed along the minor semi-axis of the ellipse (see figure 2). The formation of the damage is discussed using the stress field data obtained with the numerical simulations. By translation of the ellipse along the minor semi-axis, the crack can be linearly elongated. Its orientation can be controlled by varying the ellipse's orientation. Using this method, example shapes made of these nano-cracks are shown in figure 3.
These cracks are normally invisible in the setup used. The Rayleigh wave emitted by a laser energy deposition travel ahead of the shock wave and create a tension region, which induces cavitation bubbles on the cracks, allowing us to visualise them.

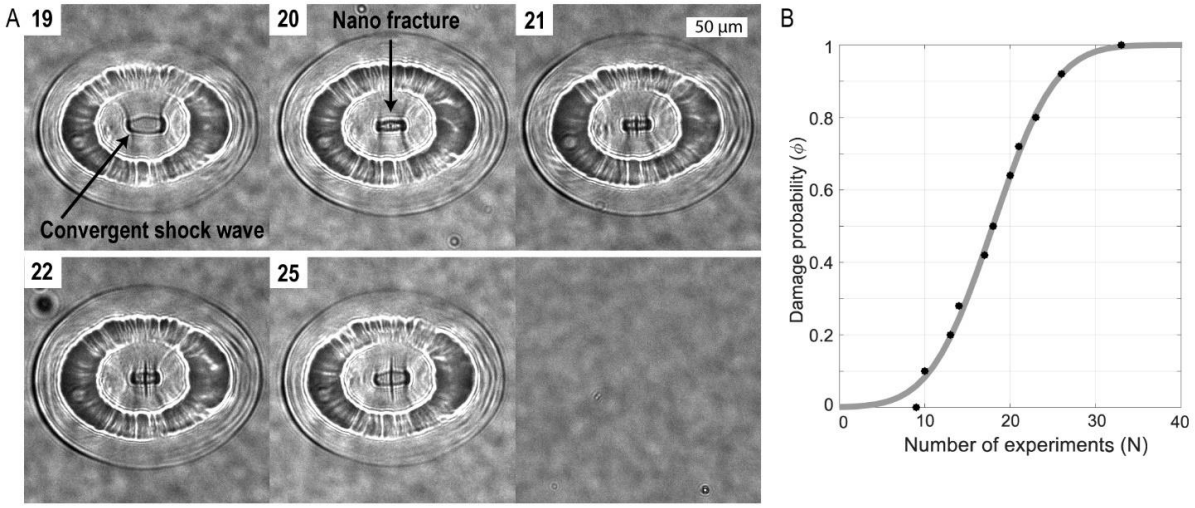

Figure 2: After several shots, a nano-crack is formed along the ellipse's minor semi-axis. The crack is only visible because it acts as a cavitation nucleus in the presence of tension induced by the emitted Rayleigh wave.

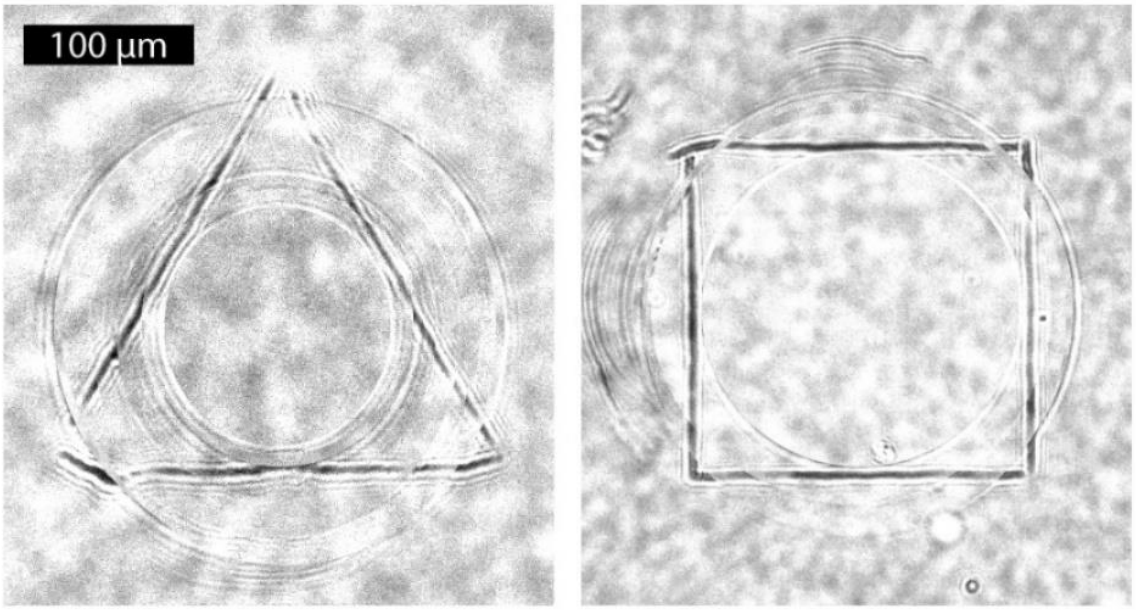

Figure 2: By translating the ellipse, a pre-existing crack can be linearly extended. By rotating it, the orientation of the crack can be controlled. This allows us to create geometric shapes out of the induced nano-cracks.

5. Conclusions

The presented methods provide a toolkit for the generation of nano-sized surface damage without direct energy deposition. They may be useful to investigate damage formation in a controlled laboratory setting, as a crack of controlled size and orientation can be induced via internal mechanical stresses without ablation as a side effect.

References

[1] U. Gutiérrez-Hernández, H. Reese, C.-D. Ohl, and P. Quinto-Su. 2022: Bullseye focusing of cylindrical waves at a liquid-solid interface, Phys. Fluids.

[2] U. Gutiérrez-Hernández, H. Reese, C.-D. Ohl, and P. Quinto-Su. 2023: Nano-Cracks and Glass Carving from Non-Symmetrically Converging Shocks, Adv. Phys. Res.

Bubble collapse at a solid boundary: influence of bubble size, liquid viscosity and ambient pressure on jet formation

Christiane Lechner[1], Max Koch[2], Matti Tervo[2],Werner Lauterborn[2], Robert Mettin[2]

[1]*Institute of Fluid Mechanics and Heat Transfer, TU Wien, Austria*
[2]*Third Institute of Physics, University of Göttingen, Germany*

1. Introduction

Jet formation in collapsing bubbles is ubiquitous whenever the setting is not spherically symmetric. For bubbles expanding and collapsing right at a flat solid boundary this asymmetry results from the viscous boundary layer that forms during the rapid expansion of the bubble. As a consequence, around maximum extension, the bubble shape deviates from a hemisphere. During collapse, flow focusing leads to cylindrically converging annular liquid inflow. For millimeter sized bubbles in water this annular inflow violently self-impacts at the axis of symmetry and leads to the formation of very fast thin axial jets [2,3,4,5]. The jet speed is of the order of 1000 m/s, exceeding the speed of the "standard" axial micro jets, that form by involution of the bubble wall, by an order of magnitude, see [1].

2. Objectives

Since fast jet formation in this setting is causally related to the viscous boundary layer, it is of interest to vary the parameters that determine the thickness of the boundary layer and quantify their influence on the jet formation process.

3. Materials & methods

We present results from numerical simulations modeling the dynamics of single (laser-generated) cavitation bubbles in axial symmetry. The model consists of a bubble filled with a small amount of non-condensable gas in a compressible liquid.
Expansion and collapse of the bubble are investigated by solving the Navier-Stokes equations discretized with the finite volume method. The volume of fluid method is used to capture the interface between liquid and gas. The model is implemented in the open source software package OpenFOAM [8].
Bubbles oscillating right at a solid boundary are considered. Bubble size, the viscosity of the liquid and the ambient pressure are varied. Configurations with high values of a bubble Weber number, $We_b = p_\infty \mathcal{R}^{eq}_{max}/\sigma$ are considered, where p_∞ denotes the ambient pressure, $\mathcal{R}^{eq}_{max}$ the maximum bubble radius and σ the surface tension coefficient.

4. Results

Results can be labeled with respect to an inverse bubble Reynolds number $1/Re_b = (\nu_l/\mathcal{R}^{eq}_{max})\,(\varrho_\infty/p_\infty)^{1/2}$, with ν_l, ϱ_∞ denoting the kinematic viscosity and the density of the liquid, and are summarized in Figure 1, see [7]. Fast jet formation is found for $1/Re_b \lesssim 0.0033$, including e.g. millimeter sized bubbles in water but also in 50 cSt silicone oil. For decreasing values of $1/Re_b$ the moment of self-impact of the annular inflow happens later and later in the bubble evolution, i.e. the bubble size at the moment of jet formation decreases with decreasing $1/Re_b$ (Fig. 1 right).
For $1/Re_b \gtrsim 0.0033$ the mechanism of jet formation changes. First a jet forms by involution of the upper bubble wall after a high curvature spherical cap has collapsed. For higher values of $1/Re_b$ a broad ``standard" micro-jet forms. The jet speed decreases monotonically with increasing values of $1/Re_b$. No jet formation is found for $1/Re_b = 6.25 \times 10^{-2}$ corresponding, e.g., to the case of a millimeter sized bubble in PAO40.

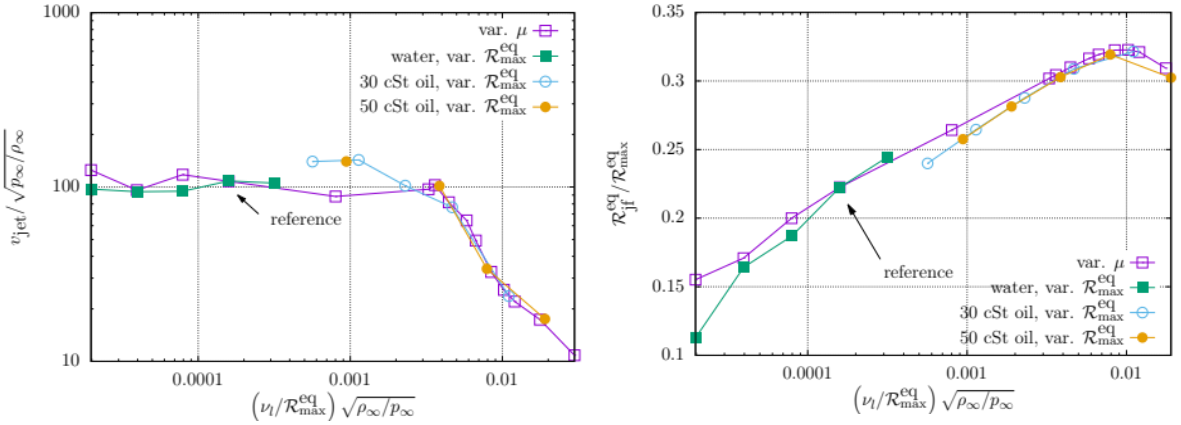

Figure 1: Jet speed (left) and bubble size at the moment of jet formation (right) as functions of an inverse bubble Reynolds number, with p_∞*=1 bar. Figures taken from [7]. The reference bubble is a millimeter sized bubble in water.*

5. Conclusions

For bubbles expanding and collapsing right at a solid boundary the formation of fast, thin jets is a very robust phenomenon. It persists also in liquids with comparatively high viscosity. The potential for erosion of the fast thin jets is under actual investigation, see e.g. [6].

When viscosity is further increased the annular inflow is damped and the jet formation mechanism changes. Although in this regime the speed of the jets is lower when compared to the fast jets, these standard jets still can impact onto the solid with a speed of several hundred meter per second and therefore might be relevant for erosion.

References

[1] A. Philipp and W. Lauterborn, J. Fluid Mech. **361,** 75–116, 1998
[2] Ch. Lechner, W. Lauterborn, M. Koch, R. Mettin, Phys. Rev. Fluids **4**, 021601, 2019
[3] Ch. Lechner, W. Lauterborn, M. Koch, R. Mettin, Phys. Rev. Fluids **9**, 093604, 2020
[4] M. Koch, J. M. Rossellό, Ch. Lechner, W. Lauterborn, J. Eisener, R. Mettin, Exp. Fluids **62,** 60, 2021
[5] F. Reuter, C.-D.Ohl, Appl. Phys. Letters **13,** 134103, 2021
[6] F. Reuter, C. Deiter, C.-D. Ohl, Ultrason. Sonochem. **90,** 106131, 2022
[7] Ch. Lechner, M. Koch, W. Lauterborn, R. Mettin, Technische Mechanik **43**, 21–37, 2023
[8] M. Koch, Ch. Lechner, F. Reuter, K. Köhler, R. Mettin, W. Lauterborn, Comp. Fluids **126,** 71-90, 2016

Cavitation Bubble Dynamics Near Brittle Boundaries

Hemant Sagar, Ould el Moctar

Institute of Ship Technology, Ocean Engineering, and Transport Systems,
University of Duisburg-Essen, Bismarckstr. 69, 47057 Germany

1. Introduction

Cavitation and their interaction with rigid boundaries, elastic boundaries, nearby various shaped boundaries, and between restricted boundaries (e.g. parallel plate) are well investigated. However, cavitation bubble interaction also exists near brittle boundaries (bone, rock, and ship fouling) and it may be applied in such cases for future application. In especially semiconductor cleaning, most silicon-based electronic components are brittle in nature. This motivated us to investigate the cavitation bubble interaction with brittle boundaries. We generated the cavitation bubble by laser focusing in water. The chalk was taken here as a brittle boundary and it was fixed to a chalk holder having a hole to firmly hold it. The bubble was generated below the chalk and in the center. We captured the bubble dynamics using the highspeed camera at a frame rate of 120Kfps and the bubble dynamics were visualized using back illumination shadowgraphy.

2. Objectives

The investigation had the following objectives:

- Preliminary study of the brittle boundary and bubble interaction
- Understanding of the brittle boundary damage by bubble collapse

3. Materials & methods

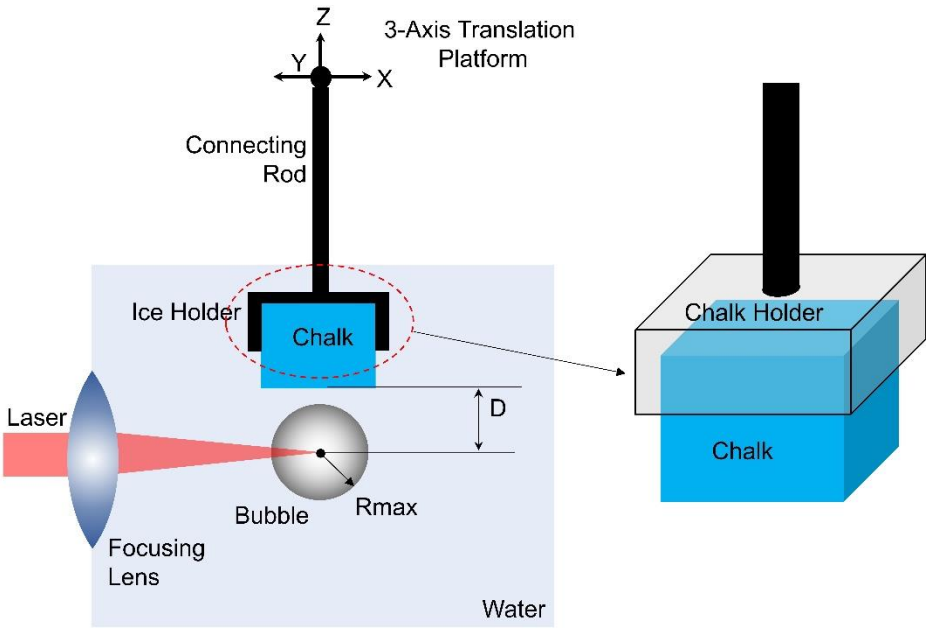

Figure 1. Experimental setup to investigate the bubble and brittle boundary interaction along with brittle material (chalk) holder configuration

Figure 1 shows the overall schematic of the experimental setup used to generate a laser-induced single cavitation bubble near the brittle boundary. Here we consider wetted chalk as the brittle boundary. Before we put chalk into the cuvette, it was kept for a few minutes in the water to absorb the water. Therefore, it did not absorb any more water from the cuvette and dissolved partially into the cuvette water. The setup consists of main equipment e.g. laser module, high-speed camera, and cuvette. The used Q-

switched, Nd:YAG laser module (Q-smart) emits the laser having a wavelength of 1064nm and pulse width of 6ns. Which further focused in the cuvette to obtain an approximate ~3mm diameter-sized cavitation bubble. Our optical system confirms the reproduction of the spherical single bubble with the probability of more than 90%. The multiple large bubble generation was almost eliminated in our experiments with distilled water. However, the chalk particles interfere with the laser path absorbing the laser energy and generating a tiny bubble near the focusing point of the laser. The bubble dynamics were captured using a highspeed camera Phantom v2012 having an Ultrafast CMOS sensor pixel size of 28 microns. We kept the framing rate of 120Kfps with an approximate period of 8.33μs and exposure time of 2μs.

4. Results

Figure 2 Illustrates the shadowgraphic imaging sequence of the bubble dynamics near brittle boundary.

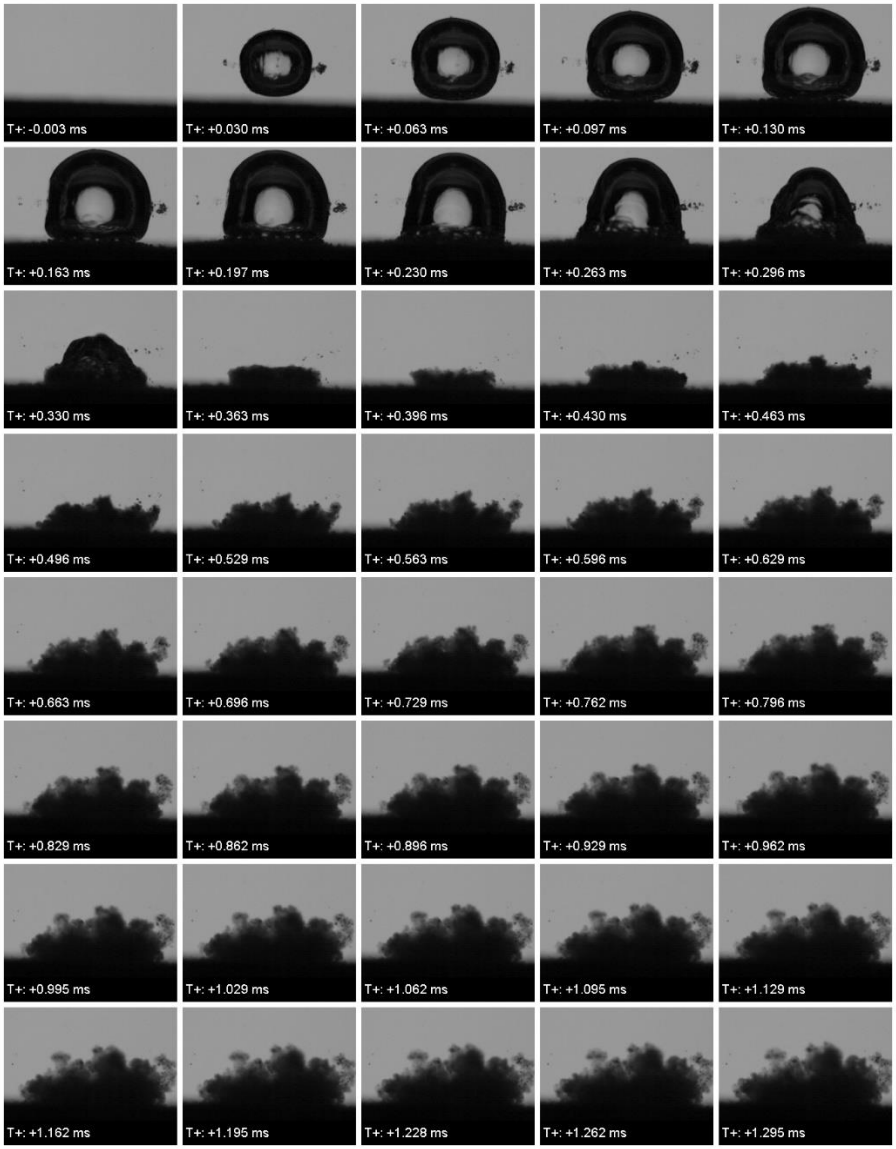

Figure 2. Bubble dynamics near the brittle boundary, here chalk.

5. Conclusions

Cavitation bubble interaction with brittle boundaries is more complex than in other cases of rigid boundaries. If the boundary is extremely brittle, a second collapse is not observed and the brittle boundary fragmentation emulsified in a way that the second collapse was almost vanished. However, the spread of the emulsification is limited to the area of bubble collapse. Our preliminary study is useful in basic understanding and developing useful applications, emulsification, and ship fouling. The challenge of simulation such a complex problem remains an open quest

Non-invasive pressure measurement on the collapse of single erosive cavitation bubbles

Fabian Reuter[1], Jaka Mur[1,2], Jernej Jan Kočica[2], Jaka Petelin[2], Rok Petkovsek[2], Claus-Dieter Ohl

[1]Otto von Guericke University Magdeburg, Institute for Physics, 39106 Magdeburg
[2]University of Ljubljana, Faculty of Mechanical Engineering, Aškerčeva cesta 6, SI-1000 Ljubljana, Slovenia

Abstract
Recently, on single bubbles it has been shown that contrary to common belief regular jetting from cavitation bubbles is not responsible for cavitation erosion on solid surfaces. Jetting even mitigates cavitation erosion as it fragments the bubble before the collapse [1,2]. Instead, cavitation is erosive through a shockwave self-focusing mechanism in which during a progressive collapse continuously emitted shockwaves converge onto a single point [1]. Details of this type of erosive bubble collapse is largely unexplored and in particular collapse pressures are unknown. They occur for nanoseconds and on micrometric scales. Therefore, a feasible route to infer the collapse pressures seems to be via measurement shockwave pressures emitted at the erosive bubble collapse. Still, collapse shockwave pressures are difficult to measure because conventional techniques using hydrophones or other sensors have a too limited bandwidth for this transient phenomenon. Furthermore, these sensors are geometrically too invasive when placed in direct vicinity to the collapse/erosion site. However, a measurement in direct vicinity of a few micrometers or tens of micrometer to the collapse site is necessary as shockwave pressures are too quickly attenuated [3].
Here, we show an optical measurement technique imaging the collapse shock front multiple times on the same image using shadowgraphy. A single erosive bubble is generated using a focused laser pulse in water close to a solid surface. Using high-magnification long working distance optics, the shock front can be imaged in direct vicinity to the collapse site. We propose a robust shock front evolution algorithm to measure the shock front propagation velocity including diffraction phenomena. From the shock front velocity, the shockwave pressure can be derived using an appropriate equation of state [4].

References
[1] Reuter, Fabian, Carsten Deiter, and Claus-Dieter Ohl. "Cavitation erosion by shockwave self-focusing of a single bubble." Ultrasonics Sonochemistry 90 (2022): 106131.
[2] Abedini, Morteza, Stefanie Hanke, and Fabian Reuter. "In situ measurement of cavitation damage from single bubble collapse using high-speed chronoamperometry." Ultrasonics Sonochemistry 92 (2023): 106272.
[3] Denner, Fabian, and Sören Schenke. "Modeling acoustic emissions and shock formation of cavitation bubbles." Physics of Fluids 35.1 (2023).
[4] Mur, Jaka, et al. "Multi-frame multi-exposure shock wave imaging and pressure measurements." Optics express 30.21 (2022): 37664-37674.

Cavitation Bubble Interaction with Compliant Structures on a Microscale

Jure Zevnik[1] and Matevž Dular[1]

[1]*Faculty of Mechanical Engineering, University of Ljubljana, Slovenia*

1. Introduction

Recent research suggests that cavitation can be used for eradication of waterborne pathogens, namely the microorganisms[1], such as bacteria and viruses. Despite the significant progress a large gap persists between the understanding of the mechanisms that contribute to the effects of cavitation and its application, which is one of the main challenges of the encompassing European Research Council project CABUM. While we are aware of some of the physical mechanisms, which are known to accompany cavitation[1]: strong shear flows, jets, high local temperatures, shock waves, and rapid pressure drop, remarkably little is known about which or a combination of which mechanisms is important for a specific consequence of cavitation. A better understanding of the fundamental physics behind the interaction between a single cavitation bubble and bacteria on a micro- and sub-microscale in thus one of the key milestones that will enable a further development of water treatment technology.

2. Objectives

The main objective of the presented work is to contribute to the understanding the fundamental physical background of cavitation bubbles in interaction with biological structures, such as bacterial cells, which could potentially facilitate a further development of water treatment technology and exploitation of cavitation in water treatment processes.

The bulk of here presented research is based on the numerical approach. Dynamics of bubbles near different structures is considered, such as rigid suspended particles, liposomes, and various types of bacteria. The focus of the studies can be divided into three main categories, which address:

- microbubble dynamics in vicinity of a deformable structure on a similar spatial scale,
- structural response to the bubble-induced mechanical loads,
- the contribution of various load mechanisms to the structural response and identification of potentially key mechanisms for bacterial cell damage.

3. Materials & methods

A fluid–structure interaction methodology is employed, where the whole domain of interest - a gas bubble, a nearby compliant structure, and ambient liquid, is split into two sub-domains - fluid and structure domain. The dynamic response of each sub-domain is solved in a separate numerical model - fluid and structure dynamics model, which are coupled together according to the partitioned iterative approach. The fluid dynamics model employs Navier-Stokes equations, which are solved according to the finite volume method along with the volume of fluid method to resolve multiphase compressible flow. Geometrical configuration of the bubble-structure pair is described with two independent dimensionless parameters, their initial distance δ and size ratio ς.

4. Results

First, the results on single cavitation microbubble dynamics in vicinity of a suspended spherical particle[2] show vastly different bubble collapse dynamics across the considered parameter space δ - ς from the development of a fast thin annular jet towards the sphere to spherical bubble collapse. The bubble jetting is much less likely to occur on the considered micro scale due to cushioning effects of surface tension and viscosity on the intensity of the collapse. The bubble emitted shock wave propagation past the spherical particle is identified as the most likely mechanical mechanism for inflicting bacterial cell damage, as shock waves exhibit large pressure peaks in the order of a few hundred MPa, gradients of 100 MPa/μm, and induce the peak shear loads of a few MPa.

Second, numerical simulations of microbubble dynamics near a liposome[3] show practically spherical bubble behavior, which points towards a negligible effect of vesicle presence on the dynamics of a nearby unattached ($\delta>1$) and similarly sized cavitation bubble. Three critical modes of vesicle deformation are identified, including uni- and bilateral bilayer extension and local wrinkling at the waist and the proximal tip of the liposome. All three are primarily driven by microstreaming during bubble collapse and rebound.

Liposomes with intact envelopes are not expected to be structurally compromised in cases with δ>1 when a nearby collapsing bubble is not in their direct contact. Regardless of the existence of past bilayer defects, liposomes are expected to be unaffected at δ >1.9. Furthermore, a higher damage potential of larger bubbles is identified.

Third, interaction between a collapsing microbubble and a nearby compliant structure that mechanically and structurally resembles a bacterial cell is addressed[4]. Across the considered δ - ς parameter space three characteristic modes of bubble collapse are identified, ranging from weak jetting away from the cell to spherical bubble collapse. The resulting peak hydrodynamic forces on bacteria range between 2 and 7 μN for more compliant gram-negative and between 10 and 22 μN for stiffer gram-positive model cells. Obtained peak local shear stresses on cell walls range between 0.5 and 5 MPa and decrease with bubble-cell sizer ratio ς. Although modes of cell deformation are qualitatively similar between both model organisms, they significantly change with ς, which is due to smaller bubbles having a more localized effect on nearby cells. Overall, four characteristic modes of spatial and temporal incidence of peak local stresses in the inner cell membrane are observed. The results show that local stresses arising from bubble-induced loads can exceed poration thresholds of cell membranes (see Figure 1) and that bacterial cell damage could be explained solely by mechanical effects in absence of thermal and chemical ones. Microstreaming is identified as the primary mechanism of bacterial cell damage, which can in certain cases be amplified by the emergence of shock waves during bubble collapse.

Finally, experimental and numerical work is brought together to study bubble-bacteria interaction on a nano- to microscale resolution in both space and time[5]. A single cavitation microbubble can cause detachment and death of wall-bound bacterial cells. In this case, a water jet resulting from a near-wall bubble implosion is the primary mechanism of cell damage. Very high likelihood of cell detachment and cell death for cells directly under the center of a bubble is observed and a peak force of 0.8 and 1.2 μN is needed for reliable detachment and death of E. *coli* bacteria.

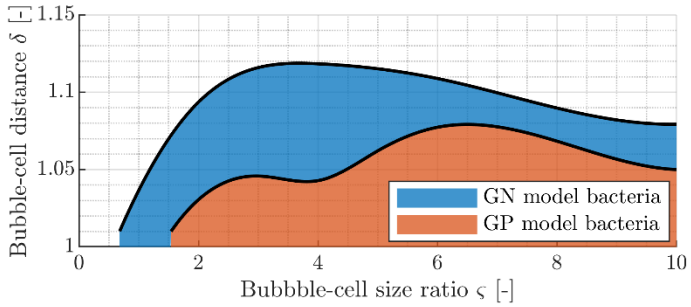

Figure 1: Estimated critical non-dimensional bubble-bacterium distances δ (solid black line) for poration of the inner cell membrane in relation to the bubble-bacterium size ratio ς. Regions in δ-ς parameter space where membrane poration threshold is exceeded are given for both Gram-negative (blue fill) and Gram-positive (orange fill) model cell.*

5. Conclusions

In an attempt to further elucidate of the process of cavitation-assisted water treatment on the fundamental level of a single bubble, the presented studies numerically address interaction between a collapsing microbubble and a nearby freely suspended structure, that mechanically and structurally resembles bacterial cells and other biological structures. A fluid-structure interaction methodology was employed, where viscous and compressible multiphase flow was considered. Numerical results were further complemented with experimental work on wall-bound E. *coli* bacteria. The results show that a single microbubble collapse event can cause bacterial cell damage, which could be explained solely by mechanical effects in absence of thermal and chemical ones.

References

[1] Zupanc, M. *et al.* Effects of cavitation on different microorganisms: The current understanding of the mechanisms taking place behind the phenomenon. A review and proposals for further research. *Ultrason. Sonochem.* **57**, 147–165 (2019).

[2] Zevnik, J. & Dular, M. Cavitation bubble interaction with a rigid spherical particle on a microscale. *Ultrason. Sonochem.* **69**, 105252 (2020).

[3] Zevnik, J. & Dular, M. Liposome destruction by a collapsing cavitation microbubble: A numerical study. *Ultrason. Sonochem.* **78**, 105706 (2021).

[4] Zevnik, J. & Dular, M. Cavitation bubble interaction with compliant structures on a microscale: A contribution to the understanding of bacterial cell lysis by cavitation treatment. *Ultrason. Sonochem.* **87**, 106053 (2022).

[5] Pandur, Ž. *et al.* Water treatment by cavitation: Understanding it at a single bubble - bacterial cell level. *Water Res.* **236**, 119956 (2023).

Optical methods for detection and evaluation of cavitation bubbles and accompanying phenomena

J. Mur[1,2], F. Reuter[2], J. J. Kočica[1], Ž. Lokar[1], J. Petelin[1], V. Agrež[1], C.-D. Ohl[2], R. Petkovšek[1]

[1]*University of Ljubljana, Faculty of Mechanical Engineering, Aškerčeva cesta 6, SI-1000 Ljubljana, Slovenia*
[2]*Otto-von-Guericke University Magdeburg, Department of Soft Matter, Universitätsplatz 2, 39106 Magdeburg, Germany*

1. Introduction

An important observable of the liquid-bubble interaction is the pressure of the shock front [1], emerging at the bubble collapse, and at generation of laser-induced bubbles. Optical measurements have proven an invaluable tool due to their non-invasiveness and their ability to measure very close to the vapor phase. Additionally, the same optical methods are suitable for evaluation of cavitation bubble dynamics and shape evolution.

2. Objectives

In the present work we combine the multi-exposure illumination technique with high-speed imaging, where each frame in the high-speed imaging series is multiple times exposed with a laser pulse much shorter than the frame exposure time. For further verification and comparison, we have used a custom designed high-bandwidth fiber-optic probe hydrophone (FOPH) [2], providing independent shock wave pressure and time-of-flight measurements. The combination allows us to precisely measure both the relatively slow evolution of the bubble shape, and faster phenomena, such as jetting and shock waves [3].

3. Materials & methods

The experimental setup, presented in Fig. 1a, was based around a custom-built short-pulse illumination system was used for imaging the cavitation bubble dynamics and the emitted shock wave. For the present study, we chose bursts consisting of four pulses with an individual pulse duration of 0.3 ns, that is sufficiently short to freeze the motion of the propagating shock wave. As a result, the shock wave is imaged four times within a frame of the high-speed camera. The time delay between pulses in a burst was varied between 5 ns and 30 ns (Fig. 1b).

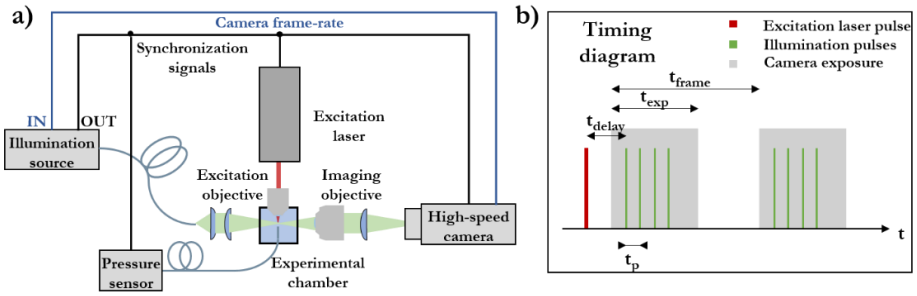

Figure 1: a) Experimental setup schematic drawing, and b) timing diagram. Synchronization timing jitter between the excitation laser pulse and the camera exposure was approx. 1 ns, and well below 1 ns between the camera exposure signal and optical illumination pulses.

A FOPH measured the transient shock wave pressure, which besides the pressure amplitude allowed to obtain the shock wave time-of-flight (TOF), i.e., the time delay between the excitation laser pulse and the shock wave front arrival on the FOPH fiber tip. The FOPH was based on a single-mode fiber as the sensing element. It was positioned perpendicular to the incident excitation laser beam direction and oriented with minimal tilt. The FOPH was mounted on a 3D positioning stage enabling accurate positioning.
The LIB was generated with an infrared nanosecond excitation laser, working at a 1064 nm wavelength with the pulse duration of 5 ns, and an available energy of 15 mJ. The laser pulse was focused in water by a lens system with NA of 0.2, resulting in a maximum bubble radius R_{max} = 1.67 mm ± 0.05 mm.
The illumination was combined with the Specialised Imaging Kirana 7M high-speed camera, operating at a 5 MHz framing rate (resolution of 924x768 pixels). The camera was used in combination with an imaging microscope objective with 10x magnification (OptoSigma, NA of 0.3).

4. Results

Automatized shock wave front recognition from camera-based images was realized in Matlab, using peak detection functions. Third order 2D-polynomial interpolation was used to achieve sub-pixel accuracy together with spatial averaging in along the shock wave front. This allowed a robust detection of the shock front, shown in Fig. 2b, and we estimate a wave front localization accuracy better than 0.3 pixels.

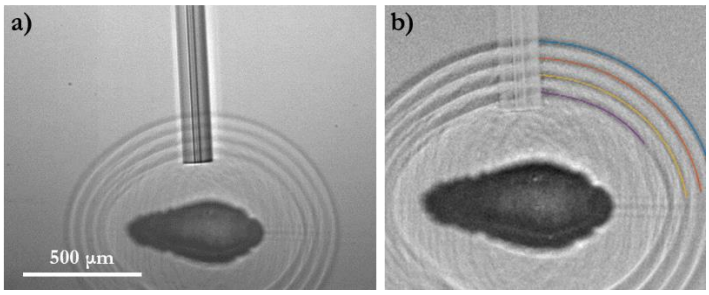

Figure 2: a) Shock waves near the initial LIB region and pressure sensor positioned nearby. The excitation laser pulse propagated from right to left. b) Improved contrast, background removed, and shock wave front recognition result.

The Fig. 3a depicts the measured pressure from the pressure sensor with a 1/r fit for comparison. These values are compared to the image-based measurements. Therefore, the shock wave velocity measurements were converted into pressure values, using the equation of state for water. The comparison of the two measurement techniques is shown in Fig. 3b. We find a good agreement of the maximum pressure for both experiments, i.e., the highest laser energies result in very similar pressures for both experiments. Yet, the pressure sensor measurements show consistent values at large distances and systematically lower pressure amplitudes at closer distances.

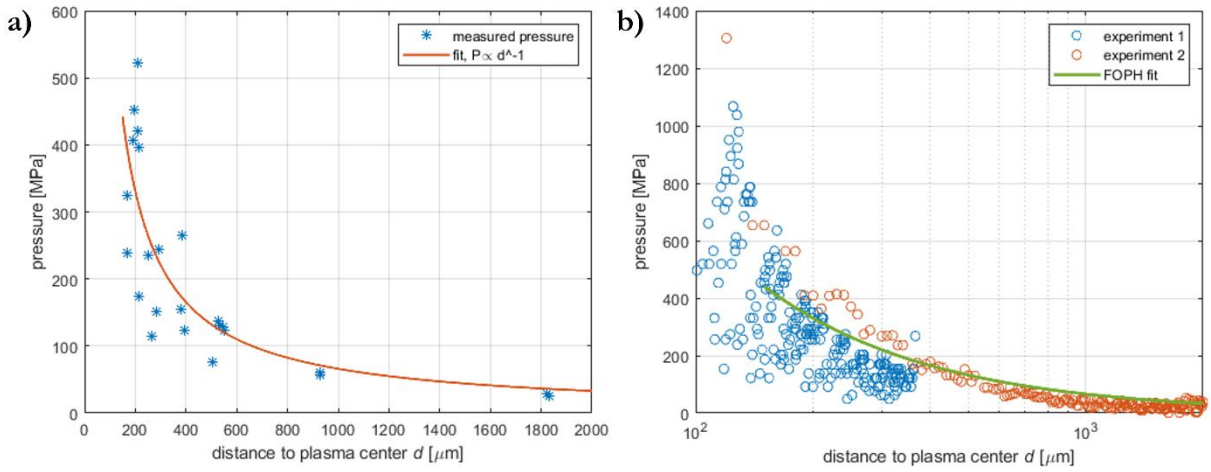

Figure 3: a) Shock wave pressures obtained from FOPH, including a guide-for-eye fit, and b) pressures from camera-based shock wave velocity measurements, converted using the equation of state for water.

5. Conclusions

A fully contactless technique of multi-frame multi-exposure imaging based on bursts of short illumination pulses is used for precise shockwave velocity measurements within a single camera frame. The measurements are verified and compared with high dynamic range FOPH pressure measurements.

References

[1] W. Lauterborn and A. Vogel, "Shock Wave Emission by Laser Generated Bubbles," in Bubble Dynamics and Shock Waves, C. F. Delale, ed. (Springer Berlin Heidelberg, 2013), pp. 67–103.

[2] J. Petelin, Z. Lokar, D. Horvat, and R. Petkovsek, "Localized Measurement of a Sub-Nanosecond Shockwave Pressure Rise Time," IEEE Trans. Ultrason. Ferroelectr. Freq. Control 69(1), 369–376 (2022)

[3] J. Mur, F. Reuter, J. J. Kočica, Ž. Lokar, J. Petelin, V. Agrež, C.-D. Ohl, and R. Petkovšek, „ Multi-frame multi-exposure shock wave imaging and pressure measurements," Opt. Exp. 30(21), 37664-37674 (2022)

Effect of cavitation microbubble on individual bacterial cells

Žiga Pandur[1], Jure Zevnik[1], Darjan Podbevšek[2], Matevž Dular[1], Stopar David[3]

[1]*Faculty of Mechanical Engineering, University of Ljubljana, Askerceva 6, 1000 Ljubljana, Slovenia*
[2]*Advanced Science Research Center at The Graduate Center of the City University of New York, 85 Saint Nicholas Terrace, New York, USA*
[3]*Biotechnical Faculty, University of Ljubljana, Jamnikarjeva 101, 1000 Ljubljana, Slovenia*

1. Introduction

Cavitation, rapid vaporization and bubble collapse due to a local change in pressure, is a widely used method in industry and research for cleaning, disinfection, dispersion, cell disruption, and isolation of cell components (1). Furthermore, it is recognized as effective and chemical free novel advanced water and wastewater treatment process (1-3). The macroscopic effects of cavitation on bacteria are the results of implosions of a large number of bubbles (1,4). However, the effects of the large bubble clusters do not reveal the inherent nature of cavitation and a plethora of possible cavitation modes of action on bacteria (mechanical, physical, chemical). As stated by Prosperetti, thousands of papers have been devoted to the subject of bubbles, yet the exact mode of action of the bubble has not been elucidated (5). To evaluate the effect of cavitation on bacteria at a fundamental level, one needs to downscale the cavitation process to a single cavitation bubble which is similar in size to a bacterial cell.

2. Objectives

Present paper addresses cavitation as a tool for eradication and removal of wall-bound bacteria at a fundamental level of a single microbubble and a bacterial cell. To do so, spatio-temporal control of a single cavitation microbubble is required, combined with a real time detection system of single bacterial cell. Furthermore, numerical analysis will help to gain additional insight into bubble dynamics and cell mechanics.

3. Materials & methods

We show the development of a new method, which enables a real time evaluation of the bacterial response to the mechanical stress induced by a single microbubble cavitation event on a nano- to microsecond time scale. With the optical tweezer we have produced a stable single nucleation bubble in the vicinity of the bacterial cell. The microbubble cavitation was triggered remotely with high voltage electric discharge which promoted pressure waves through the medium and induced nucleation microbubble growth and collapse observed with high-speed camera. Direct observation of the interaction between a single cavitation microbubble and the individual bacterial cell is presented. The evolution of the fluid flow field during the microbubble collapse was characterized by silica bead displacements, which enabled in situ measurement of the fluid velocity field during the single cavitation event. The effect of a single microbubble on bacterial cell viability was recorded by fluorescence microscopy. The experimental results were used to validate the results of the numerical model, where the evolution of the single microbubble cavitation and its interaction with a bacterial cell was simulated. The threshold wall shear stress and hydrodynamic force needed for cell detachment and bacterial death during the single microbubble cavitation event were estimated.

4. Results

Results on E. coli bacteria show that only cells in the immediate vicinity of the microbubble are affected, and that a very high likelihood of cell detachment and cell death exists for cells located directly under the center of a bubble. Further details behind near-wall microbubble dynamics are revealed by numerical simulations, which demonstrate that a water jet resulting from a near-wall bubble implosion is the primary mechanism of wall-bound cell damage. The results suggest that peak hydrodynamic forces as high as 0.8 μN and 1.2 μN are required to achieve consistent E. coli bacterial cell detachment or death with high frequency mechanical perturbations on a nano- to microsecond time scale. Understanding of the cavitation phenomenon at a fundamental level of a single bubble will enable further optimization of novel water treatment and surface cleaning technologies to provide more efficient and chemical-free processes.

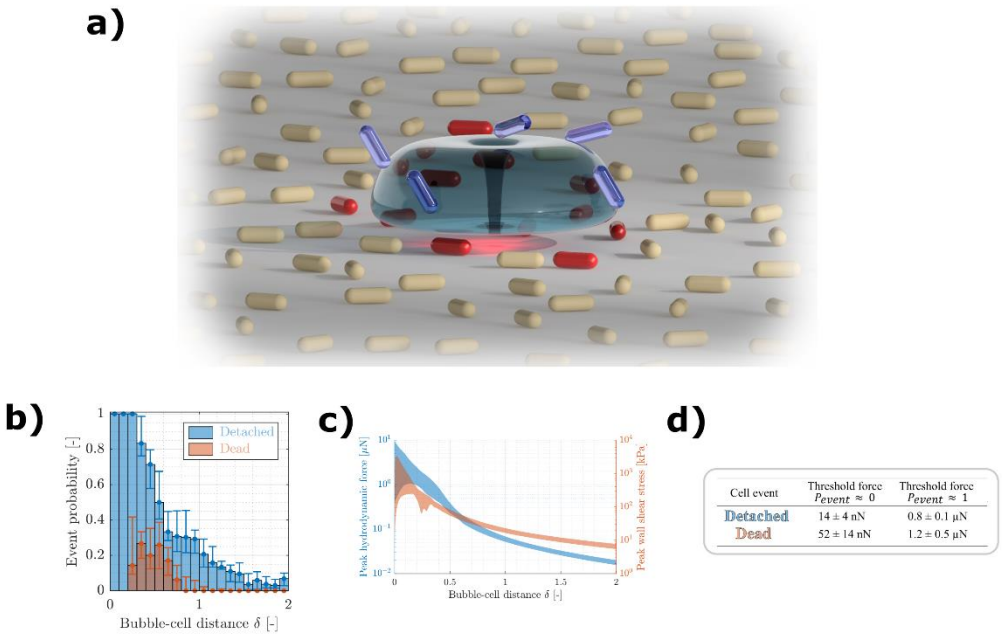

Figure 1: ***a)*** *Schematic representation of experiment where cavitation microbubble collapse occurs near rigid surface with attached bacterial cells, where typical cavitation jet occurs. At the cavitation event, some of the cells at the proximity of microbubble collapse got detached (blue colored) or their membrane integrity was compromised (red colored).* ***b)*** *Experimental results of bacterial cell event (detached or dead) probabilities in relation to microbubble-cell distance parameter δ. Blue bars represent probability of cell detachment and orange bars for cell death.* ***c)*** *Bubble numerical model shows peak hydrodynamic force (blue) and Peak wall shear stress (orange) in relation to microbubble-cell distance parameter δ for given experimental setup.* ***d)*** *Determined threshold forces for cell death or cell detachment based on experimental and numerical results.*

5. Conclusions

In this study, spatio-temporal control of a single cavitation microbubble combined with numerical analysis provided unprecedented mechanistic insight into hydrodynamic forces and shear stresses that affect individual bacterial cells during a single cavitation microbubble event. We present a direct observation of bacterial cell response to high frequency mechanical perturbations spanning the time domain from nanosecond to microsecond. The results of this study imply an intimate relation between the bacterial cell and a cavitation microbubble. Only when the two are in contact or in very close proximity, a bubble has an effect on the bacterial cell. The detrimental effect of cavitation on bacterial viability and attachment is spatially confined to the center of the projected cavitation microbubble.

References

1. Zupanc, M. et al. Effects of cavitation on different microorganisms: The current understanding of the mechanisms taking place behind the phenomenon. A review and proposals for further research. Ultrasonics Sonochemistry 57, 147–165 (2019).
2. Šarc, A., Oder, M. & Dular, M. Can rapid pressure decrease induced by supercavitation efficiently eradicate Legionella pneumophila bacteria? Desalination and Water Treatment 57, 2184–2194 (2016).
3. Zupanc, M. et al. Shear-induced hydrodynamic cavitation as a tool for pharmaceutical micropollutants removal from urban wastewater. Ultrasonics Sonochemistry 21, 1213–1221 (2014).
4. Gogate, P. R. & Pandit, A. B. A review and assessment of hydrodynamic cavitation as a technology for the future. Ultrasonics Sonochemistry 12, 21–27 (2005).
5. Prosperetti, A. Bubbles. Physics of Fluids 16, 1852–1865 (2004).

Micro-scale processes in cavitation-induced drop breakage

Deepak K. Pandey, Vivek V Ranade

Multiphase Reactors and Intensification Group
Bernal Institute, University of Limerick, Limerick V94T9PX, Ireland
**Corresponding author: vivek.ranade@ul.ie*

1. Introduction

Emulsions play a crucial role in the production of several products in the chemical, energy, and environmental industries, such as medicine, food, cosmetics etc. [1–4]. The cavitation-based techniques to produce emulsion remain one of the popular choices of these industries [2]. Cavitation results in the generation of local turbulence and liquid micro-circulation (acoustic streaming) inside the cavitation-based devices, enhancing the emulsification processes. Therefore, the microscale understanding of the collapsing cavities interacting with the other phases is of utmost importance. Several researchers have tried to explore this aspect, but few have paid attention to the micro-scale interaction of the cavities in the emulsion. Moreover, the understanding of the interaction between multiple cavities and drop(s) has not been explored satisfactorily. In this work, the microscale aspect of cavity dynamics in the vicinity of the oil drop has been explored. This includes the interaction between two cavities- a single oil drop and vice-versa.

2. Objectives

In the present work, a computational investigation is performed for the interaction of a cavity-oil drop, two cavity-single drops, and two drop-single cavity interactions. Moreover, the influence of a cavity on asymmetrical oil drop has also been explored.

3. Numerical method

A time-dependent Navier-Stokes equation for laminar flow with VOF was used to get insight into the cavity-oil drop interaction. For pressure-velocity coupling, the SIMPLE algorithm was utilized, along with implicit temporal discretization. For pressure interpolation, a second-order upwind method was adopted. Convergence criteria were 10^{-5} for continuity and momentum equations and 10^{-7} for energy equations in all situations. The adaptive mesh technique is used to refine the volume fraction gradient (up to three levels). The physical domain and boundary condition for the computational model of the considered setup is presented in Figure 1. A fine-quality mesh at the interface of the cavity-water vouches for the stability of the numerical simulation (as shown in Figure 2).

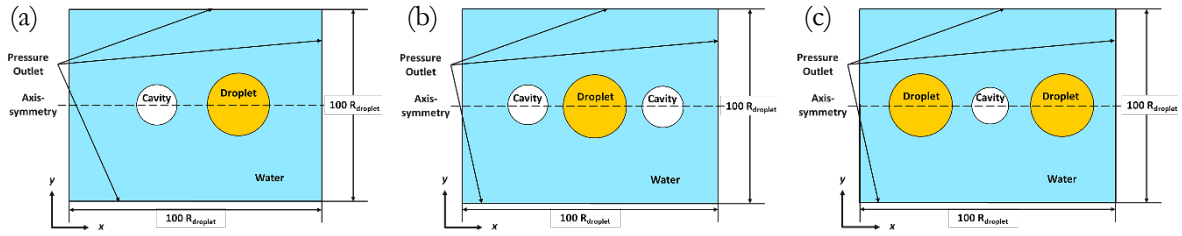

Figure 1: Schematic of the physical domain and boundary conditions for different cavity-drop configurations (a) single cavity-oil drop; (b) two cavities-oil drop; (c) two oil drop-single cavity

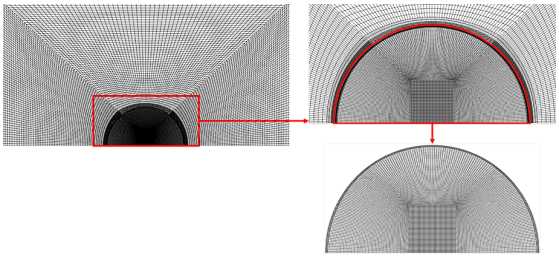

Figure 2: Computational grid of the domain

4. Results

The oscillation of a single cavity suspended in water from the numerical simulation is compared with the existing literature of Zevnik and Dular [3]. The radius oscillation result shows good agreement with the existing literature as shown in Figure 3. In the case of a cavity generated inside the continuous phase (water) and interacting with the dispersed phase (oil drop), the deformation of the oil drop [4] at the interface can be seen in Figure 4(a). Figure 4(c) shows the formation of a low-pressure region at the oil-water interface and a high-pressure region at the cavity-water interface. This generates the driving force causing the cavity to move towards the oil drop interface and try to penetrate and break the drop into several daughter drops.

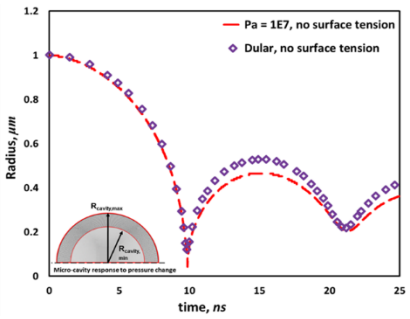

Figure 3: Cavity oscillation and its validation with existing literature

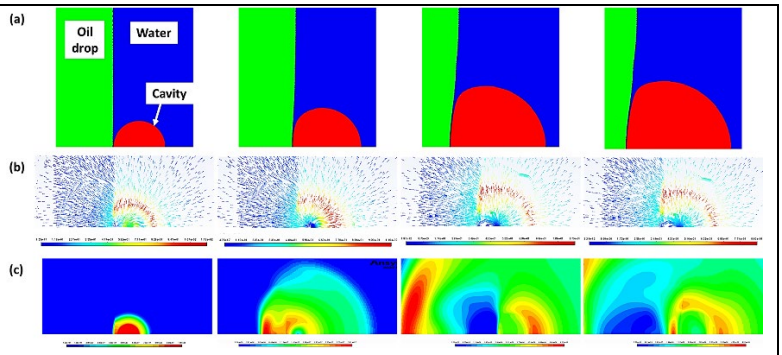

Figure 4: Cavity progression in the vicinity of oil drop (a) Phases; (b) velocity vector; (c) static pressure

5. Conclusions

Based on the present study of cavity-oil drop interaction suspended in water, we were able to get more insight into the cavity dynamics in the vicinity of the oil drop(s). Moreover, understanding of micro-scale processes related to cavitation-induced drop breakage. This insight will help in manufacturing the cavitation-based emulsion producing devices which will be more efficient.

References

[1] A. V. Pandit, V.P. Sarvothaman, V. V. Ranade, Estimation of chemical and physical effects of cavitation by analysis of cavitating single bubble dynamics, Ultrason Sonochem. 77 (2021). https://doi.org/10.1016/j.ultsonch.2021.105677.

[2] U. Orthaber, J. Zevnik, R. Petkovšek, M. Dular, Cavitation bubble collapse in a vicinity of a liquid-liquid interface – Basic research into emulsification process, Ultrason Sonochem. 68 (2020). https://doi.org/10.1016/j.ultsonch.2020.105224.

[3] J. Zevnik, M. Dular, Cavitation bubble interaction with a rigid spherical particle on a microscale, Ultrason Sonochem. 69 (2020). https://doi.org/10.1016/j.ultsonch.2020.105252.

[4] T. Stepišnik Perdih, M. Zupanc, M. Dular, Revision of the mechanisms behind oil-water (O/W) emulsion preparation by ultrasound and cavitation, Ultrason Sonochem. 51 (2019) 298–304. https://doi.org/10.1016/j.ultsonch.2018.10.003.

Single cavitation bubble dynamics and erosion in a stagnation flow

Dominik Mnich[1], Fabian Reuter[1], Fabian Denner[2], Claus-Dieter Ohl[1]

[1]Faculty of Natural Sciences, Institute for Physics, Otto-von-Guericke-University Magdeburg, Universitätsplatz 2, 39106 Magdeburg, Germany

[2]Department of Mechanical Engineering, Polytechnique Montréal, Montréal, H3T 1J4, QC, Canada

We study the dynamics and erosion of a single cavitation bubble seeded in a stagnation flow and collapsing close to a solid wall. High-speed recordings reveal rich and rather distinct bubble dynamics for different stand-off distances. While Volume-of-Fluid simulations allow numerical insight into the wall pressures and shear stresses, the material damage from multiple bubble collapses next to an aluminium sample is measured using confocal profilometry. We show that a moderate flow velocity of a few meters per second already shapes the bubble into an ellipsoid and alters the dynamics such that a planar convergent jet flow forms. This can influence the bubble-wall interaction drastically. In particular, a bubble in the small stand-off regime lifts off from the wall and the violent collapse occurs at some distance. At the same time, the shear stresses can be increased by orders of magnitude without increasing wall pressure in the same way. The results suggest that the enriched bubble dynamics may allow tailored applicability in process technology.

Experimental investigation of cavitation-induced removal of paint from the surface of the Venturi channel

Luka Kevorkijan[1*], Tilen Jernejc[1], Luka Lešnik[1], Ignacijo Biluš[1]

[1] *Faculty of Mechanical Engineering, University of Maribor, Slovenia*
[*] *Corresponding author, Luka Kevorkijan: luka.kevorkijan@um.si*

1. Introduction

In hydraulic systems cavitation is often an unwanted phenomenon. One major undesired consequence is cavitation erosion, a process that leads to further undesired consequences, such as lower efficiency of hydraulic systems and need for frequent maintenance. Different methods to predict the cavitation erosion exist. Apart from direct method of observation of cavitation erosion, different indirect methods exist, which employ a proxy material, commonly a thin metal foil [1] or a soft paint [2]. Gradually another research area has emerged, concerned with positive aspects of cavitation to exploit cavitation for example for cleaning wastewater [3].

2. Objectives

The objective of this work is to present the removal of paint due to cavitation from different materials. Depending on the material, this process is viewed as either cavitation erosion prediction or as cleaning by hydrodynamic cavitation.

3. Materials & methods

Experiments were conducted in the cavitation tunnel in the Turbomachinery laboratory at the Faculty of Mechanical Engineering, University of Maribor as shown in Figure 1. Cavitation due to a constriction of the flow cross-section was achieved in a Venturi-like channel. To obtain the Venturi-like shape of the channel, the aluminium insert was placed inside the test section made from acrylic glass, as shown in Fig. 1 b). For prediction of cavitation erosion, a paint test method was chosen, where a paint serves as a proxy to identify potential cavitation erosion zones on a metal surface. We chose the acrylic paint diluted with water, which is reported to be a good combination to be used in experiments involving prediction of cavitation erosion [2]. The paint was not applied directly to the surface of the aluminium insert. First an aluminium self-adhesive tape was applied to the relevant surface of the aluminium insert, which was then painted with a brush. This additional preparation step simplified and sped-up the overall preparation between consecutive experiment runs.

Before and after each experiment run the painted surface was scanned with an optical scanner to obtain high quality pictures from which the removal of paint was observed.

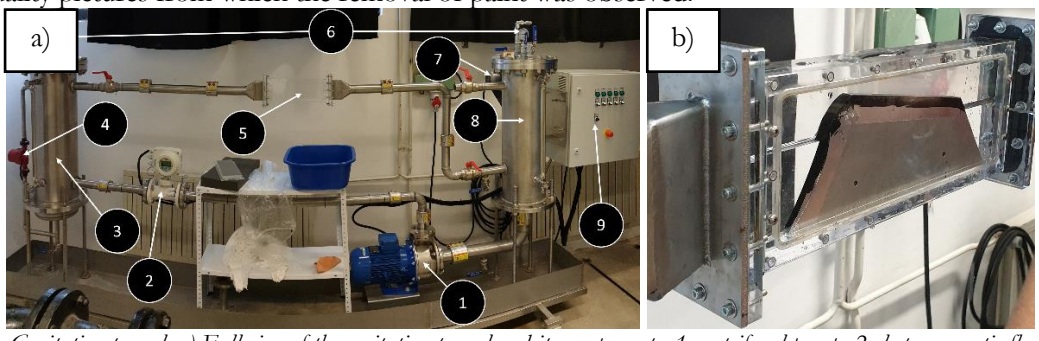

Figure 1: Cavitation tunnel: a) Full view of the cavitation tunnel and its components: 1-centrifugal pump, 2-electromagnetic flowmeter, 3-pressure tank, 4-recirculation pump, 5-test section, 6-pressure gauges, 7-vacuum pump, 8-suction tank, 9-electrobox with electromotor frequency regulator; b) Close-up view of the test section with painted aluminium insert

4. Results

In all presented results at least some removal of acrylic paint thinned with water in ratio of 1:2 was observed. All results were obtained at the same operating conditions of the cavitation tunnel, presented in Table 1.

Table 1: Operating conditions of the cavitation tunnel during experiment runs.

Volumetric flow rate [m³/h]	Cavitation number [-]	Calculated Venturi throat velocity [m/s]	Outlet static pressure [Pa]
5.78	0.77	16.06	100000

For comparison, one experiment run without paint was made with a longer time of exposure to cavitation, as shown in Figure 2 a) and b). The purpose of this experiment run was to verify, that cavitation pits do begin to form on the aluminium tape surface in the zones of paint removal.

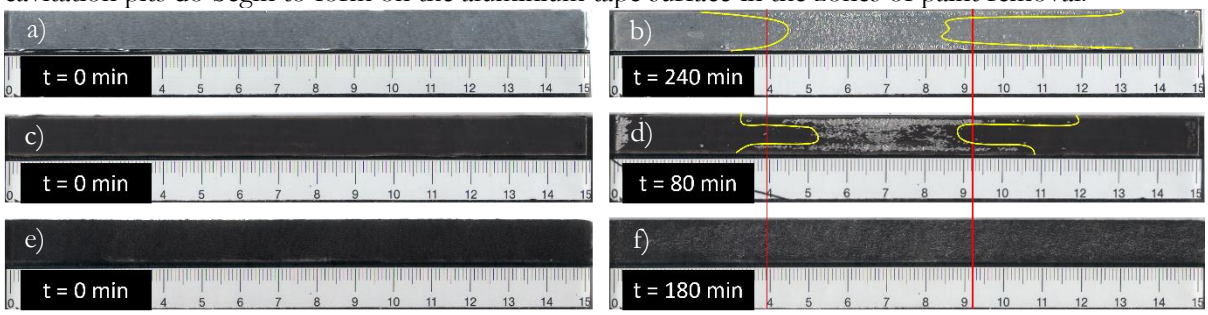

Figure 2: Results of different ecperiment runs, flow direction from left to right: a) and b) before and after experiment run with unpainted aluminium tape; c) and d) before and after experiment run with painted aluminium tape; e) and f) before and after experiment run with painted textile

There was a good agreement between results with unpainted and with painted aluminium tape, shown in Figure 2 b) and d), respectively. In both cases main zone of cavitation erosion prediction was found approximately between 4 cm and 9 cm downstream of Venturi throat, marked with red lines in Figure 2. Furthermore, in both cases a distinctive pattern, reminiscent of letter H, could be seen as drawn with yellow splines in Figure 2. Less intense removal of paint was observed in the case of painted cotton strip but over a larger area, extending upstream and downstream of previously identified zone of paint removal. A distinct pattern could not be identified. On the one hand, the removal of paint shows promise towards the use of hydrodynamic cavitation in textile cleaning applications, on the other hand, the reduced intensity compared to the aluminium surface indicates that some modifications to increase the cavitation intensity would be necessary.

5. Conclusions

Experiments to assess potential for cavitation erosion were conducted. The paint test method is found to be a suitable proxy for detecting cavitation erosion in a relatively short time. By replacing the aluminium tape with cotton strip, the research could be reformulated to explore the potential of hydrodynamic cavitation for cleaning (from previous formulation dealing with cavitation erosion). Removal of paint from cotton is achieved under the same operating conditions, however due to different results compared to aluminium tape, further work, focused on the topic of cleaning as opposed to erosion is recommended.

Acknowledgement

The authors wish to thank the Slovenian Research Agency (ARIS) for the financial support in the framework of the Research Programme P2-0196 Research in Power, Process and Environmental Engineering.

References

[1] M. Dular, and M. Petkovšek, "On the mechanisms of cavitation erosion – Coupling high speed videos to damage patterns," *Experimental Thermal and Fluid Science*, vol. 68, pp. 359-370, June 2015.

[2] B. Aktas, O. Usta, and M. Atlar, "Systematic investigation of coating application methods and soft paint types to detect cavitation erosion on marine propellers," *Applied Ocean Research*, vol 94, 101868, November 2019.

[3] M. Dular *et al.*, "Use of hydrodynamic cavitation in (waste)water treatment," *Ultrasonics Sonochemistry*, vol. 29, pp. 577-588, October 2015.

Some aspects of similarity and transferability for processes with hydrodynamic cavitation

Julius Alexander Nöpel[1], Frank Rüdiger[1]

[1]*Technische Universität Dresden, Institute of Fluid Mechanics, 01062 Dresden*

1. Introduction

Hydrodynamic cavitation is a very complex multiphase flow and the complexity increases further when it is to be used in process engineering applications. This raises the question of how the comparability of experimental results in this field can be achieved and further of how a transfer of results from laboratory experiments to an industrial process can succeed. The problem of transferability of test results for flows with cavitation has already been addressed in several publications. *Keller* (1999) summarized the influencing factors preventing a simple scaling of cavitating flows based on cavitation number into two groups. First group are the bubble dynamic effects or water quality (onset of cavitation, diffusion processes, effects from bubble motion). Second group summarizes viscosity effects and includes all factors that have an influence on the local pressure reduction (viscosity, turbulence, surface roughness, …). *Šarc* (2017) found similar results in investigations of cavitation in Venturi nozzles - the cavitation number alone is insufficient for characterizing the cavitation state. As a conclusion for future experiments, in addition to the exact description and documentation of the experimental conditions, the specification of the definition of the cavitation number and the practical determination of the quantities included in its calculation was requested. *Zupanc* (2019) summarized the current understanding of the effect of hydrodynamic cavitation on microorganisms. In doing so, they provide recommendations that should be followed to advance the research field. The requirements already mentioned are supplemented, among others, by the exact description of the treatment procedure and the determination of reactive species generated by cavitation. *Kuimov* (2023) recently investigated different Venturi nozzles and found a strongly different aggressiveness for the same values of cavitation number. The transferability was enabled by performing a regression considering significant influencing variables.

2. Objectives

Using the example of the degradation of the dye Congo red by hydrodynamic cavitation in a reactor with a cavitating free jet, the aim is to investigate the conditions under which the process is energy-efficient and how the experimental results can be transferred from the laboratory scale to an industrial scale. Congo red is used here as a representative of the group of oxidatively degradable substances. In this context, the paper focuses on the derivation of similarity indices using measured variables from the experiment.

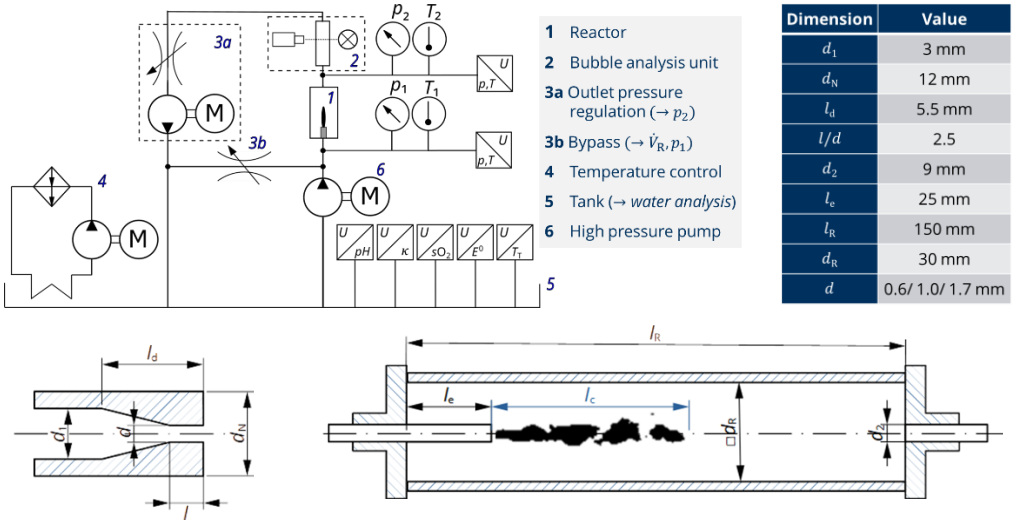

Figure 1: Experimental setup for Congo red dye degradation with hydraulic circuit diagram and dimensions of nozzle and reactor

3. Materials & methods

An experimental setup (see Figure 1) was used in which Congo red (Alfa Aesar, CAS: 521-31-3; 98 % purity), dissolved in demineralized water, is pumped in a closed circuit from a container (5) through a pump (6) via a nozzle into a reactor (1). The initial concentration of the dye was set to $c = 30$ mg/L for all cases. The treatment was performed according to a standardized procedure, starting with a circulation without cavitation until a constant concentration is reached, followed by treatment with cavitation over a period of 60 minutes, as illustrated in Figure 2. Thorough cleaning was performed between experiments, to a specified minimum concentration.

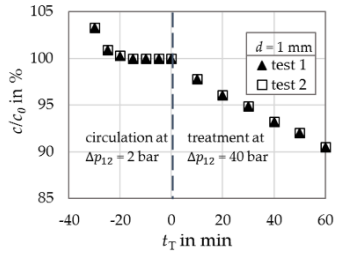

Figure 2: Exemplary change of concentration over time for standardized treatment procedure

A similarity analysis with measured process variables, the dimensions of reactor and nozzle and the oxygen saturation using Buckingham's π-theorem was conducted, giving the dimensionless complexes shown in Table 1. The oxygen saturation is used as a measure for amount of dissolved gases and so as an indicator for degassing. Further quantities of water quality have been measured but not considered in the similarity analysis yet. The complexes Π_2^{-1} and Π_3^{-1} are two different definitions of the cavitation number, Π_4^{-1} is the Reynolds number and Π_3/Π_5 gives the Weber number.

Table 1: Similarity complexes for hydrodynamic cavitation in a reactor with jet cavitation

i	1	2	3	4	5	6	7	8
Π_i	$\frac{\Delta p_{2e}}{\Delta p_{2v}}$	$\frac{\Delta p_{12}}{\Delta p_{2v}} = \frac{1}{Ka_p}$	$\frac{\dot{V}^2 \rho}{\Delta p_{2v}\, d^4} = \frac{1}{Ka_d}$	$\frac{\nu\, d}{\dot{V}} = \frac{1}{Re_d}$	$\frac{\sigma}{\Delta p_{2v}\, d}$	$\frac{\dot{V}^2 \rho_{O2}}{\Delta p_{2v}\, d^4}$	$\frac{d_R}{d}$	$\frac{l_R}{d}$

4. Results

With the standardized treatment procedure, a very good reproducibility was achieved. Figure 3 shows some exemplary results. The thorough analysis of results using the similarity complexes is the subject of recent work

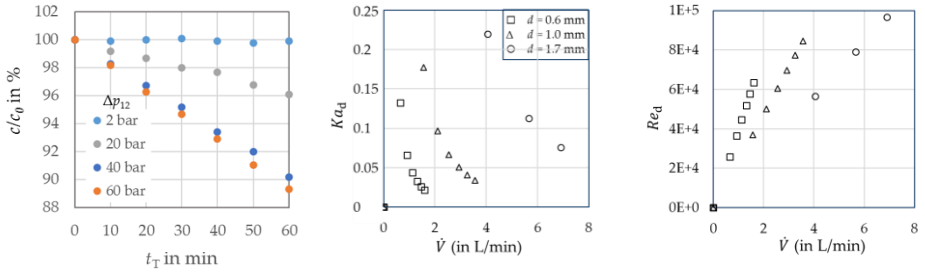

Figure 3: Degradation of Congo red dye ($d = 1$ mm, $t_T = 60$ min), $Ka(\dot{V})$ and $Re(\dot{V})$. Each point is an average of 7 tests.

5. Conclusions

Control of as many process variables as possible and a standardized test procedure are essential for correct evaluation and comparability of results. A largely open problem is the transferability of results from laboratory tests to technical processes. In particular, the water quality and the change in process and target variables usually differ greatly between these cases. This issue will be investigated next.

References

Keller, A.P., Rott, H.K., Stoffel, B., Striedinger, R.; *Maßstabseffekte bei der Strömungskavitation.* Forschung im Ingenieurwesen 65 (1999), 48-57

Šarc, A., Stepišnik-Perdih, T., Petkovšek, M., Dular, M.; *The issue of cavitation number value in studies of water treatment by hydrodynamic cavitation.* Ultrasonics Sonochemistry, vol. 34 (2017), 51-59

Zupanc, M., Pandur, Ž., Stopar, D., Petkovšek, M., Dular, M.; *Effects of cavitation on different microorganisms: The current understanding of the mechanisms taking place behind the phenomenon. A review and proposals for further research.* Ultrasonics Sonochemistry, vol. 57 (2019), 147-165

Kuimov, D. *Theoretical and experimental investigation of cavitation number limits.* E3S Web of Conferences 402, 03025 (2023), https://doi.org/10.1051/e3sconf/202340203025

Towards the concept of early detection of atherosclerosis using ultrasound contrast agent

Avinash Kumar[1]*, Dhiman Chatterjee[1], S. Vengadesan[2]

1. *Department of Mechanical Engineering, IIT Madras, Chennai 600036, India*
2. *Department of Applied Mechanics, IIT Madras, Chennai 600036, India*

**Corresponding author*

me21s040@smail.iitm.ac.in

1. Introduction

In the human cardiovascular system, the length and diameter of the left coronary artery, supplying blood to the heart muscle, is about 10-13 cm long and approximately 4-5 mm in diameter (Waller et al., 1992). Due to physiological reasons, like an increase in the level of cholesterol, plaque formation within the coronary artery takes place. In the beginning stage, plaque does not show any symptoms. This kind of plaque, also known as vulnerable or high-risk plaque, consists of 40 % lipid core (Fayad and Fuster, 2001). There are many methods to detect plaque (atherosclerosis) e.g., angiography, intravascular ultrasound imaging, etc, but these methods are quite expensive and fully invasive techniques. However, the problem of undetected atherosclerosis may lead to the death of an individual. One way to overcome this problem of accessibility of timely medical treatment is to use easily available ultrasound imaging protocol aided by the use of micro gas bubbles commonly called ultrasound contrast agents. This forms the motivation for the present work

2. Objectives

The specific objective of this work is to numerically investigate the interaction of bubbly flow inside a flexible tube, mimicking the artery, in the presence of plaque-like obstruction.

3. Materials and Method

It is known that the acoustic impedance of soft tissues (like blood vessels etc) is about 1.63 Pa.s/m, and the acoustic impedance of blood is about 1.61 Pa.s/m (Tole, 2005). The acoustic mismatch between blood vessels and blood is very low. Hence, it will be very difficult to detect plaque formation; on the contrary, the acoustic impedance of air is 0.0004 Pa.s/m (Tole, 2005).

In the present work, we carried out one-way coupled, 3-D unsteady numerical simulations of the flow of bubbles through flexible tubes mimicking the artery. The interaction of bubbly flow with acoustic irradiation is also captured in these simulations. Commercial Multiphysics software, COMSOL, was used for the purpose.

Figure 1 shows the computational domain, and Figure 2 brings out the modelled plaque region. Tables 1 and 2 give the material properties of flexible tubing and boundary conditions used in these simulations. Mechanical index of ultrasound radiation is chosen based on the usual practice in medical imaging (Şen et al., 2015).

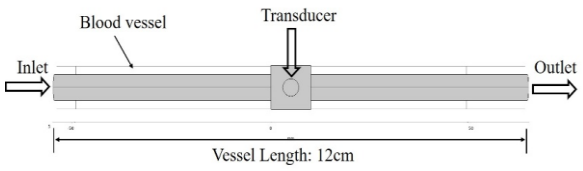

Fig. 1 Computational domain

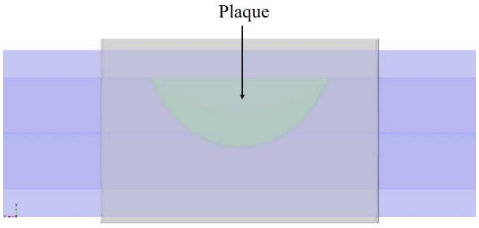

Fig. 2 Zoomed view showing the modelling of plaque

Table 1 Material properties of silicone rubber mimicking blood vessel and plaque

Silicone Rubber (blood vessels + plaque)	Young's modulus 2.97 MPa	Density 1140kg/m^3	Sound speed 1000 m/s	Poisson's ratio 0.47

4. Result

Figure 3 shows the instantaneous contour plot of velocity near the plaque region. As expected, there is an increase in velocity due to the constriction. Figure 4 shows the wall shear stress at the same

instance for which the velocity contour is shown in Figure 3. It shows regions of high wall shear stress at the leading edge of the plaque formation. This high shear stress may lead to the bursting of the plaque in a real-life scenario. Figure 5 shows a snapshot of acoustic wave transmission inside the computational domain. In Figures 3,5 the black line indicates the projection of the plaque on the plane of view. Results of acoustic pressure at a monitor location near the plaque region (as indicated in Figure 5 by a black circle) is not presented here for brevity but will be presented during the Workshop for both with and without bubbly flow case.

Table 2 Boundary and initial conditions used

water	Inlet: $v=2u_{avg}[1-(r/R)^2]$, $u_{avg}=4$ cm/s	Outlet: $P_0=100$[mmHg]	Initial Condition: $u=v=w=0$ $p=100$ mm of Hg
Air	Inlet: Gas concentration, $\varphi=0.5$	Outlet: $d\varphi/dx=0$	Initial Condition $\varphi=0$
Acoustic pressure	At the transducer source $P_{amp}=$ 1.414 MPa and frequency of 2 MHz. Mechanical index, MI, =1		

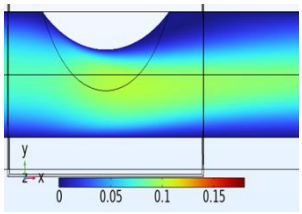

Fig. 3 Contour of instantaneou velocity magnitude near the plaque region

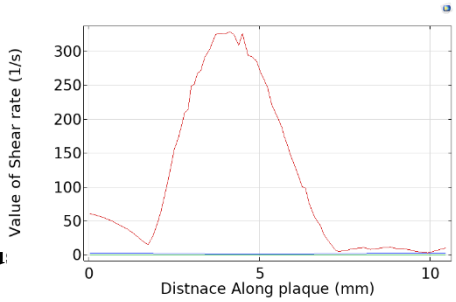

Fig. 4 Instantaneous plot of wall shear rate near the Plaque region

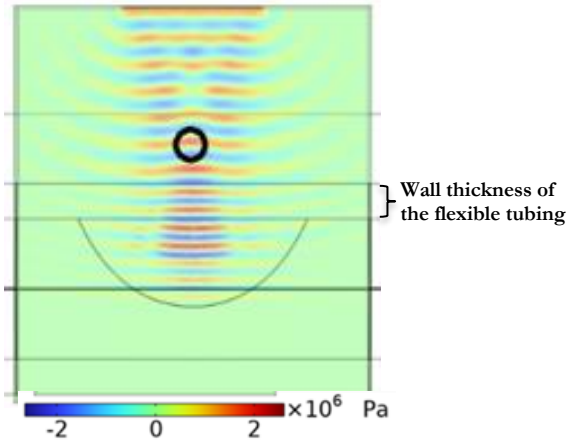

Fig. 5 Instantaneous snapshot of acoustic wave transmission. The black circle denotes the location at which acoustic pressure amplitude is monitored

5. Conclusion

When contrast agent solution is introduced to the tube, mixture fluid density and compressibility change and thereby leading to a change in the acoustic impedance of the medium. This facilitates capturing of the echo clearly and will help visualize the plaque formation.

Reference

Douglas, P.S., Fiolkoski, J., Berko, B. and Reichek, N., 1988. Echocardiographic visualization of coronary artery anatomy in the adult. Journal of the American College of Cardiology, 11(3), pp. 565-571.

Fayad, Z.A. and Fuster, V., 2001. Clinical imaging of the high-risk or vulnerable atherosclerotic plaque. Circulation research, 89(4), pp. 305-316.

Şen, T., Tüfekçioğlu1 O., Koza, Y., 2015, Mechanical Index, Anatol J Cardiol, 15, pp. 334-336

Tole, N. M., 2005. Basic Physics of Ultrasonographic Imaging by: Diagnostic Imaging and Laboratory Technology Essential Health Technologies Health Technology and Pharmaceuticals: WORLD HEALTH ORGANIZATION (Geneva).

Waller, B.F., Orr, C.M., Slack, J.D., Pinkerton, C.A., Van Tassel, J. and Peters, T., 1992. Anatomy, histology, and pathology of coronary arteries: A review relevant to new interventional and imaging techniques—Part I. Clinical cardiology, 15(6), pp. 451-457

The beginning of the ultrasonic emulsification process

Žan Boček[1], Martin Petkovšek[1], Samuel J. Clark[2], Kamel Fezzaa[2], Matevž Dular[1]

[1]*Faculty of Mechanical Engineering, University of Ljubljana, Askerceva 6, 1000 Ljubljana*
[2]*Advanced Photon Source, Argonne National Laboratory, 9700 S Cass Ave, Lemont, IL 6043, USA*

1. Introduction

A lot of effort has been dedicated in recent years towards understanding the basics of cavitation emulsification, mainly in the form of single bubbles [1–5]. Less extensive and less detailed research has been done regarding bulk acoustic emulsification [6,7], which we hope to expend with our current research. Here we focus on the onset of emulsification, as it has been reported to be the most crucial for dictating emulsion quality [8,9].

2. Objectives

The objective of our research was to visualize and characterize the behavior of oil-water interface at the beginning of ultrasound emulsification. The gained insight should be applicable not only to other types of ultrasound batch homogenization, but also to flow-through acoustic cavitation devices.

3. Materials & methods

The experiments were conducted inside 4.0mL plastic cuvettes, which were filled with 2.5mL of distilled water and 1.0mL of oil, respectively. The ultrasonic horn was positioned at various distances and locations relative to the oil-water interface (above, inside and below the interface).
For the purposes of better emulsification visualization, samples were observed with 2 highspeed cameras simultaneously, positioned at a 90°angle relative to each other. Of these cameras the first (Photron SA-Z) observed the immediate area around the ultrasonic horn and the second (Photron Mini UX100) observed the whole side of the cuvette. Analogous to observations under visible light were conducted measurements with a synchrotron under X-rays.

4. Results

An example of the resulting images from observations under visible light is shown in Figure 1. In all examples, except those where the horn was initially positioned completely inside the oil-water interface, either upwards or downwards movement of the interface towards the horn's tip had to occur before the onset of emulsion formation. These movements were most likely caused by the current created by the horn oscillation. The durations of these shifts were proportional to the initial distance between the horn and interface and, as such, took longer in examples where the initial distance was greater. As a large enough segment of the interface connected to the horn's tip, a vertical emulsion stream, roughly the width of the horn emerged from it. This formed emulsion replaced the water phase, causing the interface to further rise. During this the interface split into layers, ensuring that some of it was still connected to the horn and continuous emulsion formation could occur. The first interface movements were upwards if the horn was initially positioned above the oil-water interface and downwards if the horn's starting position was below it. However in the case of the horn being initially positioned inside the oil-water interface, onset of emulsion formation occurred quickly after the beginning of horn oscillation, without any movement of the interface.

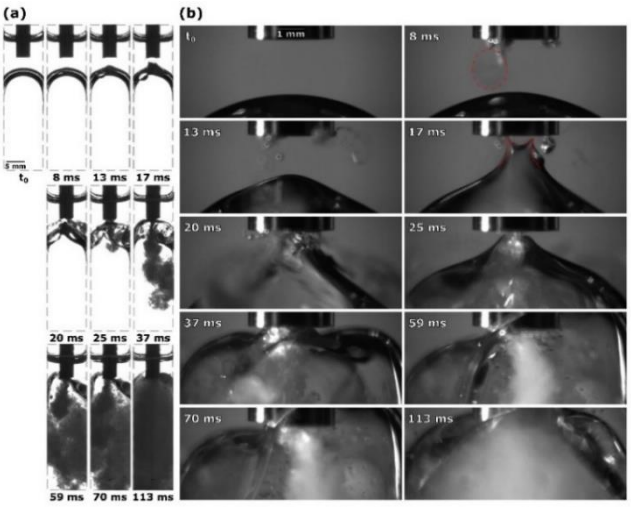

Figure 1: Sequnce of events during ultrasound emulsification under visible light with the horn positioned 2.0mm above the oil-water interface: observations with (a) Photron Mini UX100 and (b) Photron SA-Z.

5. Conclusions

The above-described findings that the interface needs to be connected to the horn's tip for an emulsion to form indicate that both a thin layer of oil and the bulk water phase need to be simultaneously present at the horn's tip (as seen in Figure 2). From this we conclude that the ultrasonic horn oscillation, specifically its downward movement "pushes" parts of the oil layer into the bulk water phase, creating a coarse oil-in-water emulsion. During the retraction of the horn, a negative pressure zone is created underneath it, causing the formation and consequent implosion of cavitation bubbles. The resulting microjets and intense local turbulences cause the break-up of larger oil droplets, leading to the formation of a finer oil-in-water emulsion. As the cycle of ultrasonic horn oscillation repeats, new oil fragments are pushed into the water phase where cavitation breaks them down. This causes the formation of the observed vertical emulsion stream. The oil layer is continuously being replenished from the bulk oil phase, therefore the presence of the oil-water interface at the horn's tip is crucial for emulsification.

Due to the oil being the less dense of the two liquids, it is always present as the upper layer and, as such, is being dispersed into the water phase, never vice-versa. This would explain why, in all observed examples, the only formed emulsion was oil-in-water emulsion, evident by the bulk oil phase remaining transparent and unchanged (only shrinking in size), while the water phase is completely incorporated into the formed emulsion and replaced by it.

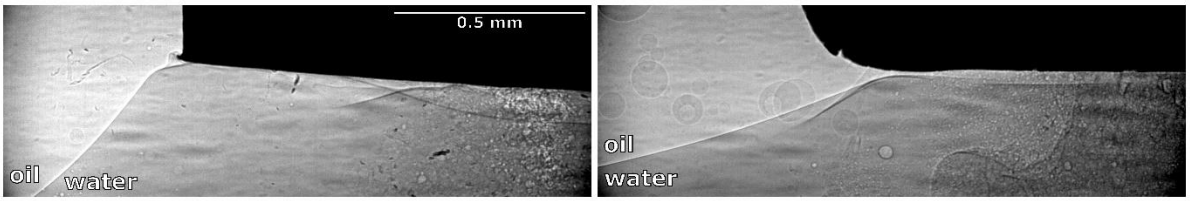

Figure 2: Observations under X-Rays of emulsion stream formation from a thin oil layer underneath the ultrasonic horn (frames taken from 2 different emulsification examples).

References

[1] U. Orthaber, M. Dular, R. Petkovšek, Characterization of jet parameters related to cavitation bubble dynamics in a vicinity of a flat liquid-liquid interface, Exp Therm Fluid Sci. 136 (2022). https://doi.org/10.1016/j.expthermflusci.2022.110651.

[2] U. Orthaber, J. Zevnik, R. Petkovšek, M. Dular, Cavitation bubble collapse in a vicinity of a liquid-liquid interface – Basic research into emulsification process, Ultrason Sonochem. 68 (2020). https://doi.org/10.1016/j.ultsonch.2020.105224.

[3] T. Yamamoto, S. V. Komarov, Liquid jet directionality and droplet behavior during emulsification of two liquids due to acoustic cavitation, Ultrason Sonochem. 62 (2020). https://doi.org/10.1016/j.ultsonch.2019.104874.

[4] R. Han, A.M. Zhang, S. Tan, S. Li, Interaction of cavitation bubbles with the interface of two immiscible fluids on multiple time scales, J Fluid Mech. 932 (2022). https://doi.org/10.1017/jfm.2021.976.

[5] K.A. Raman, J.M. Rosselló, H. Reese, C.D. Ohl, Microemulsification from single laser-induced cavitation bubbles, J Fluid Mech. 953 (2022). https://doi.org/10.1017/jfm.2022.971.

[6] T.J. Tiong, J.K. Chu, L.Y. Lim, K.W. Tan, Y. Hong Yap, U.A. Asli, A computational and experimental study on acoustic pressure for ultrasonically formed oil-in-water emulsion, Ultrason Sonochem. 56 (2019) 46–54. https://doi.org/10.1016/j.ultsonch.2019.03.026.

[7] A. Cucheval, R.C.Y. Chow, A study on the emulsification of oil by power ultrasound, Ultrason Sonochem. 15 (2008) 916–920. https://doi.org/10.1016/j.ultsonch.2008.02.004.

[8] B. Abismail, J.P. Canselier, A.M. Wilhelm, H. Delmas, C. Gourdon, Emulsification by ultrasound: drop size distribution and stability, 1999. https://doi.org/10.1016/S1350-4177(98)00027-3.

[9] S. Kentish, T.J. Wooster, M. Ashokkumar, S. Balachandran, R. Mawson, L. Simons, The use of ultrasonics for nanoemulsion preparation, Innovative Food Science and Emerging Technologies. 9 (2008) 170–175. https://doi.org/10.1016/j.ifset.2007.07.005.

A hybrid Eulerian-Langrangian CFD model for predicting cavitation intensity

Suat Canberk Ozan[1*], Pascal Müller[2], Jan Hendrik Cloete[1]

[1] *Flow Technology Department, SINTEF Industry S. P. Andersens veg 15B, NO-7031, Trondheim, Norway*
[2] *Department of Mechanical Engineering, ETH Zurich, D-MAVT Leonhardstrasse 21, 8092 Zurich, Switzerland*
**canberk.ozan@sintef.no*

1. Introduction

When the liquid pressure temporarily drops below the vapor pressure, either due to the hydrodynamics created by the flow geometry or through acoustics, cavitation occurs. Although the intense shockwaves, pressures and temperatures generated by the collapsing cavitation bubbles render the phenomenon undesirable in many configurations, it is also possible to exploit these extreme conditions to intensify processes such as micropollutant removal in wastewater treatment where the radicals produced during the collapse of the cavitation bubbles play a key role. The complex geometries (such as an impeller or an orifice plate) involved, as well as the significantly different time and length scales, make the modelling of cavitating flows challenging and often computationally expensive. Therefore, the majority of the existing theoretical studies either focus on the dynamics of a single bubble within a stagnant liquid phase (or under extremely simplified flow conditions) or employ cavitation models that neglect some of the important bubble-scale physics for the sake of computational efficiency. Although the cavitation models currently available in common CFD software successfully estimate when and where cavitation occurs, they cannot predict the bubble trajectories throughout the rest of the domain or the collapse conditions, i.e., temperature and pressure, which is of crucial significance to process intensification efforts. To address this issue, we propose an alternative hybrid Eulerian-Lagrangian approach for cavitation modelling with CFD that is capable of capturing the drastic dynamic changes in the bubble properties both during their growth and collapse, thereby yielding key information that were previously unavailable within typical CFD simulations.

2. Objectives

This work focuses on proposing a new CFD simulation framework that couples bubble- and flow-scale-dynamics for better estimation of cavitation dynamics by combining Lagrangian particle tracking with Euler-Euler multiphase flow simulations. The main goal of the proposed framework is to predict the cavitation bubbles' trajectories within the hydrodynamic flow device, as well as to reveal the bubble collapse conditions (e.g., temperature, pressure, radical production rate) that are inaccessible in Eulerian cavitation closures. Besides the CFD framework, this work also studies the changes in the bubble chemistry under the extreme collapse conditions by considering isolated bubbles subject to acoustic cavitation.

3. Materials & methods

ANSYS Fluent 2021R2 is employed in the CFD simulations. The description of the main solution algorithm is presented in Fig. 1: Following the initialization, the Euler-Euler multiphase solver is run (with Schnerr-Sauer cavitation model enabled). Upon convergence, discrete particles (bubbles/nuclei) are injected and tracked throughout the cavitation device by using the built-in Lagrangian tracking capability of ANSYS Fluent. This built-in capability is substantially customized via user-defined functions to integrate the single bubble dynamics (SBD) equations that govern the bubble size, temperature, pressure, and chemical composition. The SBD model used here is an adaptation of the diffusion-limited model proposed by Toegel et al. (2000) combined with the reaction kinetics suggested by Kamath et al. (1993) (or with equilibrium calculations). The SBD is a set of ordinary differential equations that consists of the Keller-Miksis equation, mass and energy balances across the bubble interface, and the overall energy balance for the bubble. Verification of the SBD model and the subsequent study on the bubble collapse chemistry and the reaction kinetics are carried out in Python.

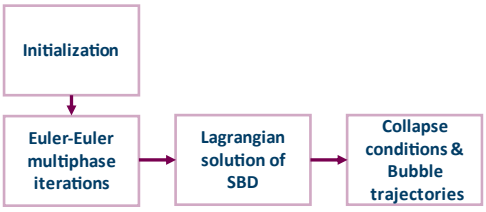

Figure 1: Description of the solution algorithm

4. Results

To test the procedure and the model capabilities, a simple cylindrical channel with a single 1mm-orifice is considered. The computational domain is 2D axisymmetric and the nuclei content injected into the channel at the inlet has a uniform size distribution of 10 microns. The inlet and the outlet pressures are 6 bar and atmospheric, respectively. The bubble trajectories colored by their diameters, temperatures, and pressures are presented in Fig. 2.

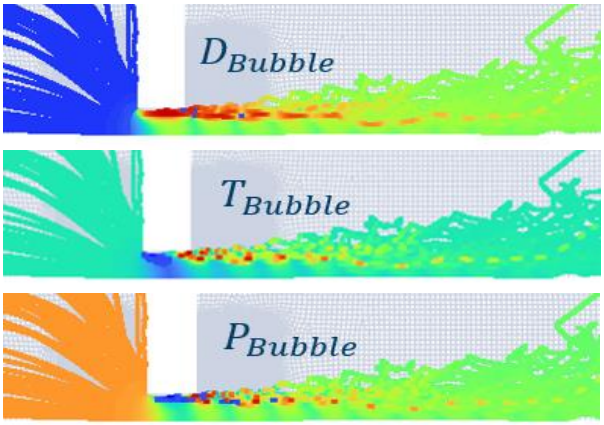

Figure 2 : Bubble trajectories colored by bubble size (10-42 microns), temperature (150-1250K), and pressure (0.06-37 bar). Blue represents the minimum and red the maximum on the color scale.

The simulations show that the bubbles grow over 50 times by volume during the cavitation process and reach a maximum temperature of 1250K and pressure of 37 bars during their collapse. All three properties begin oscillating significantly once the cavitation bubbles leave the low-pressure zone. The oscillations are dampened as flow progress, yet they are visible well after a few millimeters from the exit of the orifice. Although such oscillations are well-known and previously discussed in works focusing on SBD (e.g., Capocelli et al, 2014), the flow and the geometries handled in these works are extremely simplified. Observing such an oscillatory behavior in more realistic flow scenarios or obtaining detailed information on the key bubble properties (such as their extended trajectories) has not been possible through built-in cavitation models in the common CFD software. As accurate prediction of the bubble chemistry relies heavily on the instantaneous values of the bubble temperature, pressure and composition, the proposed algorithm carries the potential to improve the understanding of processes that rely on the exploitation of the radicals produced during bubble collapse.

5. Conclusions

A new approach for cavitation modelling through CFD simulations is proposed. The approach integrates Lagrangian particle tracking enhanced by the SBD model into Euler-Euler multiphase simulations. The results imply that it is possible to predict size, pressure, and temperature of the cavitation bubbles, as well as their oscillations as a function of time, which has not been possible through the conventional cavitation models in CFD software. Having access to such information in CFD simulations can potentially improve the current understanding of processes where particle collapse conditions play an important role and lead to formation of models/expressions with higher predictive power.

Acknowledgments

The authors would like to acknowledge funding received from the Research Council of Norway (project number: 329127) as part of the Eurostars program (project E! 115526 HYDROCAT).

References

Toegel, R., Gompf, B., Pecha, R., & Lohse, D. (2000). Does water vapor prevent upscaling sonoluminescence?. Physical review letters, 85(15), 3165.

Kamath, V., Prosperetti, A., & Egolfopoulos, F. N. (1993). A theoretical study of sonoluminescence. The Journal of the Acoustical Society of America, 94(1), 248-260.

Capocelli, M., Musmarra, D., Prisciandaro, M., & Lancia, A. (2014). Chemical effect of hydrodynamic cavitation: simulation and experimental comparison. AIChE Journal, 60(7), 2566-2572.

ACCOMPANYING PROGRAM

WEDNESDAY, 20th of September at 19.00

GALA DINNER at Ljubljana castle

THURSDAY, 21st of September at 18.30

SIGHTSEEING of Ljubljana

Meeting point: PREŠERN SQUARE